Author response to reviewer 1

The authors response is shown in red
Changes implemented in the new version of the manuscript are in blue

We thank the reviewer for the comments, which we consider very important. Here our response to each of them.

More motivation for the presented work should be included. For example, I was wondering how accurate current IEC-recommended methods for estimating loads in waked conditions are, and if there is a clear need to improve these methods using lidar-measured wind conditions. Additionally, I was wondering why the authors did not compare the accuracy of the load predictions to the accuracy when using these IEC standard wake modeling methods. It was not until the end of the paper (last paragraph of Section 5) that these topics were discussed. I believe this material should be moved to the introduction to better motivate the research and to explain the scope of the current work (i.e., that comparison with DWM, etc. is not part of the current work).

Following the comment of the reviewer, we now provide further motivation on the need to improve load validation approaches in wakes, and clarify the scope of the work along the manuscript. Further, "Sect. 2.1 Requirements for load validation in wakes" is fully dedicated to define the scope of the current work and introduce the reader with the elements of the load analysis.

The following text is added on page 2 line 9:

The comparison of fatigue loads predicted using the DWM and the effective turbulence approach by the IEC showed a discrepancy of 20% (Thomsen et al., 2007). The uncertainty varied according to the inflow conditions and spacing between turbines. The work of Larsen et al. (2013) showed a very fine agreement between both power and load measurements and predictions based on a site-specific calibrated DWM model for the Dutch Egmond aan Zee wind farm. However, the study did not quantify uncertainty in a systematic approach. More recently, Reinwardt et al. (2018) estimated fatigue load biases in the range 11–15% for the tower bottom and 8–21% for the blade-root flapwise bending moments using the DWM. To date, these approaches are characterized by a significant level of uncertainty, due to the stochastic nature of environmental conditions and the various simplifying assumptions used in the wake model definitions (Schmidt et al., 2011). Further, these results motivate the need for improving wind turbine load validation approaches in wake conditions.

The following replacement is done in the abstract on page 1 line 4:

From: "We account for wake-induced effects by means of wind field parameters commonly used as inputs for load simulations, which are reconstructed using lidar measurements."

To: "The wake flow fields are described by lidar-estimated wind field characteristics, which are commonly used as inputs for load simulations, without employing wake deficit models."

The following text is added in the introduction on page 2 line 21:

Based on these findings, we extend the load validation procedure defined in Dimitrov et al. (2019) to include wake conditions. Therefore, wake-induced effects are accounted for by means of wind field parameters commonly used as inputs for load simulations, which are reconstructed using lidar measurements, yet without employing wake deficit models.

-Many of the paragraphs throughout the manuscript are very long, often an entire page. Organizing them into smaller paragraphs would greatly improve the readability. For example, pg. 2, pg. 11, pg. 14, pg. 17.

To improve readability, we restructured the manuscript as following:

- Section 4.1 Wake effects on reconstructed wind parameters
- Section 4.2 Wake effects on turbulence spectra properties

We renamed section 4.3 from "Load simulation results" to "Load validation procedure" and re-arranged the section 4.3 as:

- Section 4.3 Load validation procedure
- Section 4.3.1 Power predictions
- Section 4.3.2 Extreme load predictions
- Section 4.3.3 Fatigue load predictions

"Sect. 4.4 Sensitivity analysis" is now divided in:

- Sect. 4.4 Sensitivity of inflow parameters on load predictions
- Sect. 4.4.1 Uncertainty distribution as function of wind speed

Specific comments:

1) Pg. 1, ln. 10: ": : :lead to an increase of the relative error as low as 4%" Kind of a confusing sentence. Maybe something like "only increase the relative error by 4% in some cases"?

The following text is modified in the abstract on page 1 lines (10)

From: "Compared to the reference case, the simulations in wake conditions lead to an increase of the relative error as low as 4%"

To: "Compared to the free-wind case, the simulations in wake conditions lead to increased relative errors (4–11%)."

2) Pg. 2, ln. 2: "To account for these effects, aero-elastic load simulations are combined with wake models: : :" How are lifetime fatigue loads calculated? Are the fatigue loads with and without the added wake turbulence/wake models added together, weighted by the frequency of occurrence for waked and freestream conditions?

In our opinion the current best practice is to derive lifetime fatigue loads based on site-specific conditions, e.g., using mast measurements, if available, or assuming appropriate probability distribution of the wind conditions at the site. With knowledge of the ambient conditions and the wind direction distribution in relation to the wind farm layout, the lifetime fatigue loads can be derived by weighting the frequency of occurrence of waked and free-stream conditions. Here, we derive the 1-Hz damage equivalent load for each 10-min period, without computing lifetime fatigue loads. However, the proposed approach could also provide information on the frequency of occurrence of waked and free-stream conditions and it can be extended to derive lifetime fatigue loads.

3) Pg. 2: The lidar literature review is very concentrated on the activities of DTU Wind Energy. DTU is certainly one of the leaders in lidar for wind energy, but including more works from other organizations would make a more representative review. As an example, a couple other relevant references are:
-Turbulence: Newman, J. F. and Clifton, A.: An error reduction algorithm to improve lidar turbulence estimates for wind energy, Wind Energy Science, 2017.
-Wakes: Iungo, G.V.; Porté-Agel, F. Volumetric Lidar Scanning of Wind Turbine Wakes under Convective and Neutral Atmospheric Stability Regimes. J. Atmos. Ocean. Technol. 2014.

The recommended references are now added.

4) Table 1: Can you explain the difference between u_{hub} (mean wind speed at hub height) and U (in the TI definition)? Or are these the same and could be written with the same symbol?

We now replace the U with u in Table 1 and throughout the manuscript.

5) Section 3.1: A figure showing the coordinate system and variables would be helpful.

The coordinate system and orientation of the axis can be derived from Fig. 2 and the definition of the angle is self-explanatory in the text. As the manuscript is already quite long, we added a figure showing the coordinate system and the variables in the appendix.

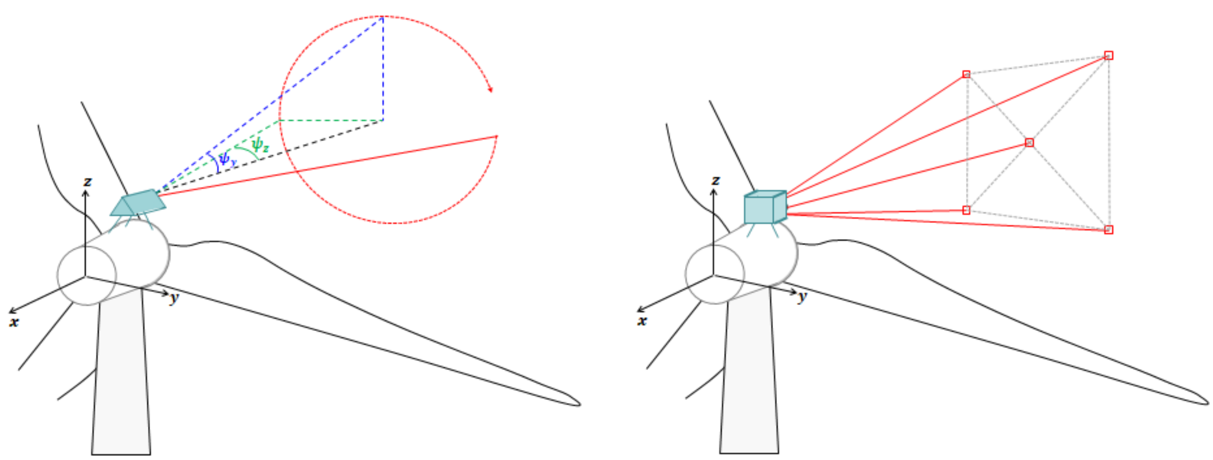

6) Eq. 4+5: Please explain the meaning of a 3D LOS vector. The component along the lidar beam direction makes sense, but what are the other two components?

The T_{LOS} is a 3x3 rotational matrix obtained from the product of two rotations about the y- and z-axes, ψ_y and ψ_z (see figure above). The 1st row of T_{LOS} defines the transformation between the LOS (along the beam of the lidar) and the reference-coordinate system (x,y,z) of figure above.

Theoretically, the 2nd and 3rd rows of T_{LOS} would refer to the transformation between two vectors perpendicular to the LOS and the reference system. As the lidar measures only the LOS, then only the 1st row of T_{LOS} is used.

In order to clarify this, we correct the manuscript and specify that only the 1st row of T_{LOS} is used before introducing Eq. 5.

The following text is added on page 7 line 8 before Eq. 5:

As lidars measure only the LOS velocity, the first row alone of T_{LOS} is considered. The relation between the wind vector and the LOS velocity is expressed in terms of matrix transformations as:

$$\boldsymbol{u_{los}} = \boldsymbol{T_{LOS} T_1 u}. \tag{1}$$

7) Eq. 6: Should C_{ind} only be applied to the first term in the brackets, aligned with the rotor orientation (the direction of the rotor thrust)? This is how it is written in Dimitrov et al. 2019. Additionally, a little more information about C_{ind} would be useful for the reader. What are the input parameters to C_{ind}?

Eq. 6 is now corrected.

The following text is added on page 7 line 16:

The two-dimensional induction model assumes longitudinal and radial variation of the induced wind velocity. The resulting induction factor C_{ind} is computed as:

$$C_{ind} = \left[1 - a_0 \left(1 - \frac{\xi_x}{\sqrt{1+\xi_x^2}}\right) \cdot \left(\frac{2}{\exp\left(+\beta_a \epsilon_a\right) + \exp\left(-\beta_a \epsilon_a\right)}\right)^2\right], \tag{2}$$

where a_0 is the induction factor at the rotor center area; $\xi_x = x/R_{rotor}$ is the distance from the rotor normalized by the rotor radius; $\rho_a = \sqrt{y^2+z^2}/R_{rotor}$ is the radial distance from the rotor center axis; $\epsilon_a = \rho_a/\sqrt{\lambda_a(\eta_a + \xi_x^2)}$, where $\gamma_a = 1.1$, $\beta_a = \sqrt{2}$, $\alpha_a = 8/9$, $\lambda_a = 0.587$, $\eta_a = 1.32$ (Dimitrov et al., 2019).

8) Pg. 7, ln. 17: "The parameters (u_{hub},: : :" Because of the induction zone model, I imagine the induction factor is also a parameter that is estimated. Is this true?

This is correct, the C_{ind} is now included in the sentence.

9) Pg. 7, ln. 28: "The velocity fluctuations, denoted by u = (u,v,w), are expected homogenous: : :" Shouldn't it be that the "statistics" of the velocity fluctuations are expected homogeneous?

We corrected and added "statistics" in the sentence.

10) Eq. 7: Should R be a function of the separation vector r?

R is defined as the covariance tensor. R(r) is a function of the separation vector when computing a two-point turbulent statistics, where the selected two points are separated by a vector

r. However, for single-point turbulent statistics r=0, the covariance tensor (R(r=0) = R) can be expressed in matrix form that contains variance and covariance terms of the wind field u=(u,v,w).

To clarify, the following text is replaced on page 7 line 28:

From: "The velocity fluctuations, denoted by u = (u,v,w), are expected homogeneous in space (Mann, 1994). The covariance tensor of single-point turbulent statistics can be written as:"

To: " The velocity fluctuations (u', v', w'), where $(')$ denotes fluctuations around the mean value, are expected homogeneous in space (Mann, 1994). It follows that the auto- or cross-covariance function between two points can be defined only in terms of the separation distance as $R_{ij}(\boldsymbol{r}) = \boldsymbol{u}'_i(\boldsymbol{x})\boldsymbol{u}'_j(\boldsymbol{x}+\boldsymbol{r})\rangle$, where i, j = (1,2,3) are the indices corresponding to the components of the wind field, $\langle\rangle$ denotes ensemble averaging, and $\boldsymbol{r} = (r_1, r_2, r_3)$ is the separation vector in the three-dimensional Cartesian coordinate system. The covariance tensor of single-point turbulent statistics $(\boldsymbol{R}(\boldsymbol{r} = 0) = \boldsymbol{R})$ can be written as:

$$\boldsymbol{R} = \begin{bmatrix} \langle u'u' \rangle & \langle u'v' \rangle & \langle u'w' \rangle \\ \langle v'u' \rangle & \langle v'v' \rangle & \langle v'w' \rangle \\ \langle w'u' \rangle & \langle w'v' \rangle & \langle w'w' \rangle \end{bmatrix} = \begin{bmatrix} \sigma_u^2 & \sigma_{uv} & \sigma_{uw} \\ \sigma_{vu} & \sigma_v^2 & \sigma_{vw} \\ \sigma_{wu} & \sigma_{wv} & \sigma_w^2 \end{bmatrix}, \tag{3}$$

11) Eq. 8: R_i, j should be a function of r here, not k.

This is now corrected.

12) Pg. 9, ln. 24: "The relation between the covariance matrix of the LOS is then: : :" It seems something is missing here. The relationship between the covariance matrix and what else?

The following text is replaced on page 9 line 24:

From: "The relation between the covariance matrix of the LOS is then expressed in terms of σ_u^2 as:"

To: "The relation between the covariance matrix of the LOS components and that of the undisturbed wind field is then expressed in terms of σ_u^2 as:"

13) Eq. 13: I believe this equation results in a matrix. How do you go from a matrix to a scalar value used to scale the LOS variance?

R_{LOS} is the full covariance matrix containing three vector components: the LOS and the other two vectors perpendicular to the LOS. However, as lidar measures only the LOS component, only the first component of R_{LOS} is measured. Therefore the ratio in Eq. 13 defines the relation between the LOS variance (as scalar) and the variance of the u-component.

The following text is replaced on page 9 line 26:

From: "Since only LOS velocities are measured by the nacelle-mounted lidar, the ratio in Eq. (13) identifies the relation between the LOS variance and the wind field variance in the longitudinal direction"

To: "Note that R_{LOS} is expressed as a full covariance matrix containing three vector components. However, as only LOS velocities are measured by the nacelle-mounted lidar, only the first component of R_{LOS} is measured. It follows that the ratio in Eq. (14) identifies the relation between the LOS variance and the wind field variance in the longitudinal direction"

14) Pg. 10, lns. 4-6: The full details can be left to Pena et al. 2017, but a little more detail about how the different beam directions are combined to find the u-component variance would be appreciated, since "computing the variance of Eq. (5)" is hard to interpret.

We added the equation below, which shows the relation between the LOS variance and the variance of the u-component. The equation is derived from the extended form of Eq. 5 by applying the variance operator. In its extended form, as shown in Peña et al. 2017, the LOS variance and the lidar orientation angles are known variables, while the variances $\langle u'u' \rangle$,$\langle v'v' \rangle$,$\langle w'w' \rangle$ and covariance $\langle u'w' \rangle$ are unknown. As the measurements of the CW lidar are grouped in 10 bins within each range, we require minimum four of these bins to solve the system and derive the variance of the u-component. This is valid under the assumption of homogenous turbulence.

The following text is now added on Page 10 lines 4-6:

By assuming homogeneous turbulence, we use the scanning pattern to account for cross-contamination of different velocity components and extract 10-min σ_u^2 statistics by computing the variance of Eq. (5) as:

$$\mathrm{Var}(u_{los}) = \mathrm{Var}\left((\cos\psi_y \cos\psi_z \cos\varphi - \cos\psi_y \sin\psi_z \sin\varphi)u - (\cos\psi_y \cos\psi_z \sin\varphi + \cos\psi_y \sin\psi_z \cos\varphi)v + (\sin\varphi)w\right) \tag{4}$$

By solving the variance operator and neglecting the resulting terms $\langle u'v' \rangle$ and $\langle v'w' \rangle$, as explained above, σ_u^2 is derived as shown in Eq. (10) in Peña et al. (2017).

15) Pg. 10, ln. 8: "The filtered turbulence derived from CW and PL lidars are plotted: : :" Which beams are used to derive the turbulence?

To derive the filtered turbulence estimates from both the CW and PL lidars, we used all the beams and ranges. To derive the unfiltered turbulence from the CW lidar, we use only measurements at 1.3 D.

We replaced the text in the manuscript on page 10 line 8:

From: "The filtered turbulence derived from the CW and PL lidars are plotted respectively in Fig. 4 (left and middle), whereas the unfiltered turbulence derived from the CW lidar is shown in Fig. 4 (right)."

To: "The filtered turbulence derived from CW and PL lidars, using all the ranges and beams, are plotted respectively in Fig. 4 (left and middle), whereas the unfiltered turbulence derived from the CW lidar measurements at 1.3 D are shown in Fig. 4 (right)."

16) Pg. 11, ln. 27: "The conservative thresholds ensure a strong wake influence in the inflow conditions: : :" This seems like a good approach for this study, but using the algorithm for a full load validation would probably miss some of the more benign wake conditions. Would this lead to overestimating the wake loads if only the strong wake conditions are simulated?

The conservative thresholds ensure the strong impact of wakes on the 10-min measured/simulated wind field and wind turbine statistics. As we run the uncertainty quantification separately for partial-, and full-wake conditions, this approach allows us to identify and differentiate the conditions within the 10-min periods. Further, as the uncertainty increases for wake situations compared to the free case scenario, we indeed expect these results to be on the conservative side.

17) Pg. 12, ln. 5: ": : :through the PL and CW lidar-estimated wind speed, turbulence and shear exponent in Fig. 6." Is Eq. 6 used to find the wind parameters, or another method? Since Eq. 6 combines multiple ranges together to estimate the wind field parameters, I'm guessing you are using a different approach here.

We corrected and rephrased the text. In the analysis shown in Fig. 6, we investigate how the lidar-based wind characteristics varies as function of the upstream ranges in free, partial- and full-wake situations. For this particular analysis, we disregard induction effects.

The following text is now added on page 12, line 5:

From: "We observe these effects through the PL and CW lidar-estimated wind speed, turbulence and shear exponent in Fig. 6. Here, the slope of a linear regression model between the free wind mast-measured and lidar-estimated wind parameters in free-, partial- and full-wake situations are shown as function of the upstream distance from the rotor."

To: "Here, the slope (m) of a linear regression model between the free wind mast-measured and lidar-estimated wind parameters in free-, partial- and full-wake situations is shown. In this particular analysis, the lidar-based wind parameters are derived from Eq. (6) evaluated a different upstream distances from the rotor without including induction effects."

18) Pg. 12, ln. 9: "while the mast is wake-free": How are you determining if the mast is wake free? For example, from Fig. 1, at 265 degrees, the mast looks like it will be waked.

Some details were described on page 11 line 19. However, we now add an Appendix to describe the application of the wake detection algorithm to the mast measurements.

Appendix A: Wake detection from mast measurements

The wake detection algorithm (see Sect.3.4) is extended to the mast measurements to classify 10-min periods where the mast is in free or wake situations. For this purpose, turbulence observations from the cup anemometer at 80 m and vertical wind shear computed using the measurements from the cup anemometers at 57.5 and 80 m are used as wake detection parameters. Their $99th$ percentiles are used as conservative thresholds to characterize the limits of the normal range of the site-specific free wind conditions. The resulting thresholds are $TI_{mast,99} = 0.20$ and $\alpha_{mast,99} = -0.02$. If one of the two limits is exceeded within a 10-min period, the mast is considered in wake conditions and shown with green markers in Fig. 1.

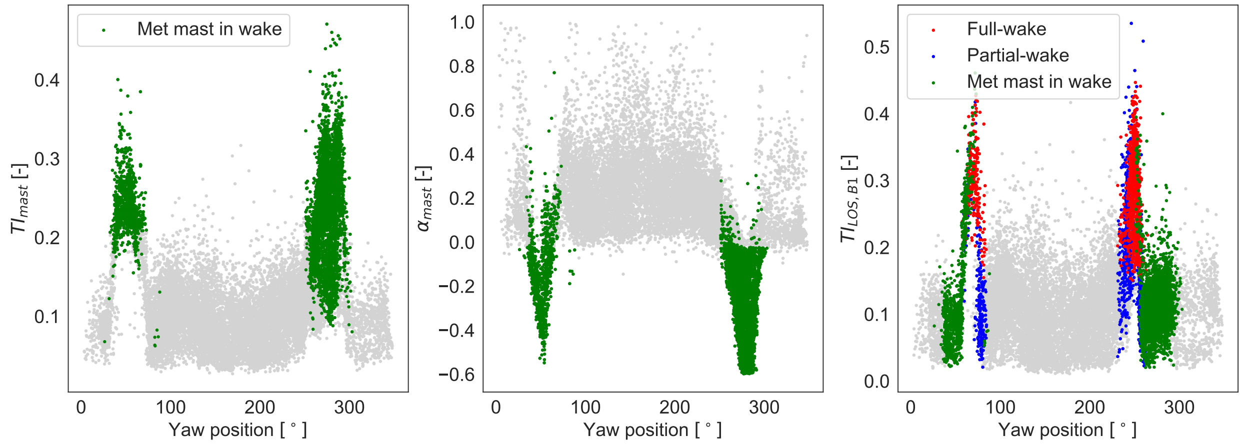

Figure 1: Left and middle: 10-min observations of the turbulence intensity and vertical wind shear at the mast as function of turbine yaw position. Free wind conditions relative to the mast are identified with grey markers, and waked situations with green markers. Right: PL-estimated 10-min wake detection parameter $TI_{LOS,B1}$. Detected wake situations of turbine T04 are shown with coloured markers: wake-free (grey), partial-wake (blue) and full-wake (red). The 10-min periods, where the mast is affected by wakes are shown in green markers.

19) Pg. 13, ln. 3: ": : :shows low bias at farther beams": Please clarify what you mean by low bias in this case. Bias between the two types of lidars?

The following text is replaced on page 13 line 3:

From: "The inter-comparison between PL and CW filtered turbulence in wake situations shows low bias at farther beams, where larger probe volume averaging effects are expected for the CW lidar (Dimitrov et al., 2019)."

To: "The difference between PL and CW filtered turbulence in wake situations (circle and star markers) decreases at farther beams, where larger probe volume averaging effects are expected for the CW lidar (Dimitrov et al., 2019)."

20) Pg. 14, ln. 29: "Small-scale turbulence is also responsible for increasing the width of the Doppler spectrum." Can you explain how the turbulence scale impacts the Doppler spectrum width? I would expect this to be a function of the standard deviation, but it isn't clear how the length scale directly impacts this.

The small-scale (high frequency) fluctuations will be filtered out by the probe volume of lidar measurements, especially if the characteristic turbulence length scale is lower than the probe volume size. However, the analysis of the Doppler radial velocity spectrum can recover information of the turbulence at the different scales. It is expected that small-scale turbulence from wakes result in broadening of the Doppler spectrum compared to ambient flow conditions. The widening of the Doppler spectrum relates to increased variance (or standard deviation) of the LOS velocity. These effects were reported in Held and Mann (2019).

21) Pg. 14, ln. 32: "It can be noticed that broadening effects are present only in b3: : :" Where is the evidence of broadening effects? Wouldn't this require the velocity spectrum in freestream conditions for comparison?

We added the Doppler spectrum for a wake-free case with similar inflow conditions.

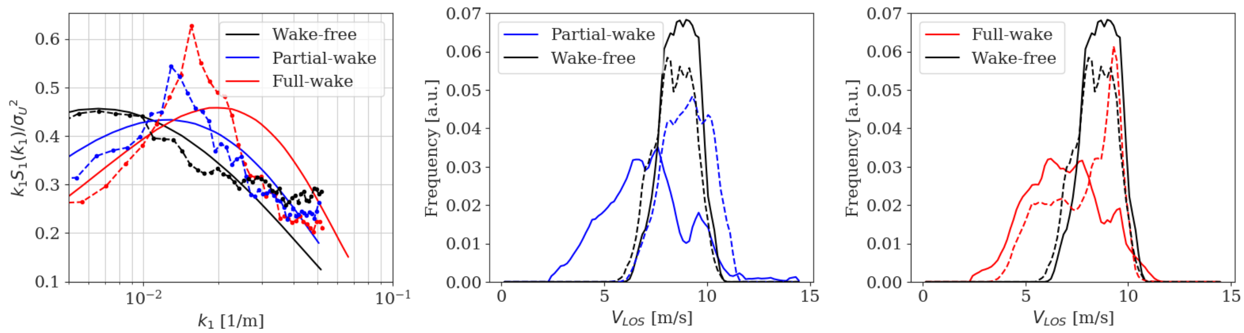

We replaced the following text on page 14 line 29-32:

From: "Small-scale turbulence is also responsible for increasing the width of the Doppler spectrum (Branlard et al., 2013; Held and Mann, 2019). We show an example of a 10-min ensemble-average Doppler spectrum obtained from the radial velocity of the CW lidar using bins b3 and b8 (see Fig. 2 for notation) at 1.3 D in partial-wake and full-wake in Fig. 7 (middle and right). The relative free wind speed measured at the met mast is 9 m/s.

To:" The small-scale turbulence generated within wake flows generally leads to a significantly larger broadening of the Doppler spectrum compared to that in the ambient flow (Branlard et al., 2013; Held and Mann, 2019). We show an example of a 10-min ensemble-average Doppler spectrum obtained from the radial velocity of the CW lidar using bins b3 and b8 (see Fig. 2 for notation) at 1.3 D in partial-wake and full-wake in Fig. 7 (middle and right). We also provide the ensemble-average Doppler spectrum in free wind for reference."

22) Pg. 15, ln. 18: Please compare with the coefficient of determination equation in Dimitrov et al. 2019. It appears there are some typos in the equation listed here.

The coefficient of determination is now corrected

23) Pg. 16, ln. 5: Why is only MXBCmin investigated, as opposed to MXBCmax?

This is due to the convention used in the strain gauges. The increasing flapwise bending moment results in negative loading. We keep the same convention as in (Dimitrov et al., 2019).

24) Pg. 17, ln. 8: "DeltaR / DeltaR,Ref": Should this be "DeltR - DeltaR,Ref"? Or "DeltaR / = 104%"?

We perform comparisons between indicators from different cases and refer to the relative error between the load uncertainty in free wind conditions and wake situations. Therefore, it should be interpreted as DeltaR - DeltaR,Ref. We corrected the text accordingly.

25) Pg. 17, ln. 10: "induction effects are dominant at these ranges: : :" Doesn't the WFR in Eq. 6 already account for induction effects to estimate the freestream (or in this case wake) wind speed?

We corrected and replaced the sentence to:

The power predictions deviations in partial-wake drop to approximately 1%, when the PL lidar-estimated wind characteristics using measurements up to 1.3 D are used in the simulations. This result indicates the sensitivity of the reconstructed wind field characteristics to the upstream ranges in a strongly inhomogeneous wind field as a partial-wake situation.

26) Pg. 17, ln. 17: ": : :as low as 3%": Should this be "as high as 3%"? This seems to be the highest % over DeltaR,Ref, not the lowest.

We added the signs in text to differentiate between over and underestimation and also specified in the text if it is under- or over-prediction.

27) Pg. 18, ln. 7: "The obtained linear regression coefficients for Power: : :" This is a nice analysis. Are the trends the same for MXBCmin and MXTBDEL (which aren't shown)?

We show the linear regression coefficients for all the channels in the figure below.

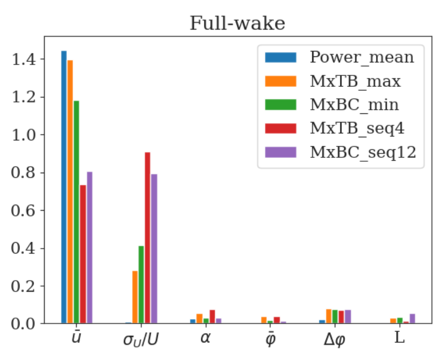

28) Table 3: It would probably be worth repeating the (short) caption from Table 2 here.

This is now done as suggested.

29) Pg. 19, ln. 1: ": : :slightly higher sensitivity of L in full-wake compared to partial wake and free-wind conditions." The partial wake loads still show a strong dependence on L (although less than full wake). Any thoughts on why the regression coefficient for L is almost zero for partial wake?

The results in Fig. 10 should be interpreted as the coefficients of a linear regression model between the inputs and the output sensors. The regression models are fitted to a dataset of 850 10-min periods, which are characterized by different inflow conditions (i.e. wind speed, turbulence, shear, etc.) as measured by the PL lidar and the L parameter, which was varied between the defined boundaries (see figure below for the partial-wake). Note that we show the absolute input values in the figure, although the inputs are normalized such that their values are scaled between zero and one, when fitting the regression model. The resulting coefficients give an estimation of the slope of a linear model between inputs and outputs. If a strong dependency is seen between output and inputs, as for the mean wind speed and turbulence in the figure below, a strong sensitivity of output sensor to the input is indicated. In the case of L, we do not see a linear relationship, but rather a scatter plot. This is because, while we vary L, the wind speed and turbulence levels are also varied, and the impact of the latter two is higher to that of L. However, when all inputs are fixed and only L varies, as the results in Table 2 and Table 3, we can estimate the effective influence of L on the predictions.

There might be several reasons why the regression coefficient for L in partial-wake is lower than that for full-wake. One is explained above. Another reason is that the absolute values of the coefficients depends on the dataset used. In fact, we use different data for the partial- and full-wake. A third one is that the L parameter is varied between 15 and 30 m for partial-wake, but between 7-30 m in full-wake.

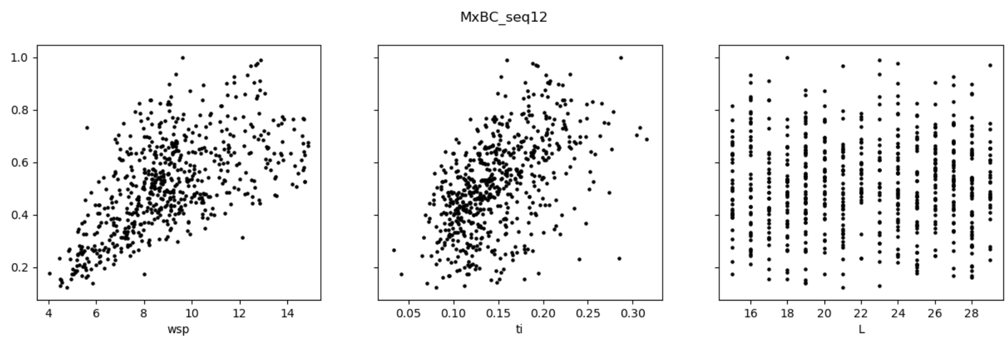

Figure 2: Scatter plot of the normalized fatigue loads at the blade-root as function of inflow wind conditions (mean wsp, turbulence and turbuelence length scale L)

30) Pg. 23, ln. 7: "Further investigation is necessary to verify that the observed uncertainty of predictions are comparable with results using state-of-the-art wake models: : :" How would this be investigated? Would you need freestream measurements of the inflow conditions to use as inputs to the wake model? If so, how would the freestream conditions be measured, given that the mast appears to be waked for much of the sector where the turbine is waked?

The intention is to state that the observed uncertainty based on the proposed method is comparable to that from IEC wake models/approaches. The dataset at the NKE site could be potentially used to quantify the uncertainty of load predictions based on the, e.g., DWM model. As the reviewer mentioned, the validation should be limited to directions and the statistics where the mast is wake-free. Other dataset could also be used for this analysis. For example, the SWiFT experiment at Sandia provides high spatial and temporal resolution lidar measurements of the wake flow field and concurrent measurements of the ambient flow from a meteorological mast. We are currently analysing SWiFT experiment data.

Author response to reviewer 2

The authors response is shown in red
Changes implemented in the new version of the manuscript are shown in blue

We thank the reviewer for the comments, which we consider very important. Here our response to each of them.

Summary: Upstream measurements of nacelle-mounted Doppler lidars are used to characterize the inflow wind field of a wind turbine and to set-up simulations for load and power predictions. These predictions are then validated by:
(i) quantifying uncertainty indicators between lidar-based prediction and measurements of onboard sensor in waked conditions
(ii) comparing uncertainty indicators quantified between mast-based prediction and on-board sensors in free wind conditions with the results of (i).
Lastly, the sensitivity of the results to the input parameters of the load simulation is investigated. It is concluded that using lidars for load and power validations is a viable possibility, but further research is needed to compare with IEC standards.

General comments: The manuscript motivates the research question and its relevancy. The methods describe the measurement site, the scan set-up of the lidars, and their processing in sufficient detail, but is scant with information on the simulation and the on-board sensors. My main issues with manuscript are (explained in more detail in the specific comments below):

1. The same inflow parameters that are used to characterize a free-stream inflow are applied to a waked inflow without modification. This includes the assumption of a power-law wind profile that is not valid within a wake.

We agree that the power law is not valid in wake conditions. The vertical wind speed gradient in wakes can be seen as the combination of the atmospheric shear, which can typically be described by a power-law profile, and the wake deficit. However, due to the complexities of wakes, i.e., horizontal and vertical meander and, at NKE in particular, scenarios with multiple wakes the velocity gradients are very complex. It would be very complicated to separate each effect from lidar measurements, without tracking the wakes' center locations in time and without knowing the wake-free atmospheric shear. With the current setup, the derived wind characteristics anyway minimize the error between the modelled wind field and lidar measurements. Fitting a power law on these data is equivalent to applying a low-order approximation to a complex nonlinear function, effectively there is minimal difference between using the average value and the power law. As shown from the the sensitivity analysis in Fig. 10, the shear exponent does not have a significant impact on the predictions. The results from Table 2 and Table 3 as well as those in Fig. 10 and Fig. 11 indicate a higher load predictions uncertainty in wakes compared to free wind conditions. As we assume that the observed deviations in load predictions are solely due to the error in the wind field representation (see Page 3 line 20), it can be inferred that the increased uncertainty is due to the flow modelling assumptions of the used wind field model. This was stated and discussed in the discussion section (see Page 21 line 9-19). In addition, we have made changes in multiple relevant parts of the manuscript, to outline the caveats of using a power law together with wake deficits.

We think that an improved scope of the work is required as well as an extended discussion regarding the limitations due to the modelling assumptions. We therefore replaced or added text:

Page 1 line 4:

From: "We account for wake-induced effects by means of wind field parameters commonly used as inputs for load simulations, which are reconstructed using lidar measurements."

To: "The wake flow fields are described by lidar-estimated wind field characteristics, which are commonly used as inputs for load simulations, without employing wake deficit models."

Page 1 line 13

From: "Finally, the experiences from this study indicate that characterizing turbulence inside the wake as well as defining a rotor equivalent wind speed model are the most challenging aspects of load validation in wake conditions."

To: "Finally, the experiences from this study indicate that characterizing turbulence inside the wake as well as defining a wind deficit model are the most challenging aspects of lidar-based load validation in wake conditions."

The following text was added in the introduction on page 2 line 21:

Based on these findings, we extend the load validation procedure defined in Dimitrov et al. (2019) to include wake conditions. Therefore, wake-induced effects are accounted for by means of wind field parameters commonly used as inputs for load simulations, which are reconstructed using lidar measurements, yet without employing wake deficit models. The objective of this study is to demonstrate how loads in wake conditions can be predicted accurately, quantify the uncertainty, and compare it to the uncertainty of mast-based load assessments in free wind.

The following text was replaced in the the discussion on page 21 lines (9-19)

From: "Although the present work does not focus in details on the performance of the two lidar systems, the findings indicate that the main sources of uncertainty in load predictions are related to flow modelling assumptions. Power production levels are highly dependent on the estimated mean wind speed at hub height. The observed power prediction's deviations, in both partial- and full-wake situations, indicate an inaccurate reconstruction of the mean wind speed. More precisely, the flow modelling assumptions, including horizontal homogeneous wind flow, power law vertical wind profile and linear veer within the scanned areas, introduce larger errors in wake than wake-free conditions. Furthermore, we do not distinguish situations where the lidar beams are partly measuring inside the wake and partially outside to reconstruct the inflow wind field. This could be resolved if wake characteristics as shape, depth and center position are integrated in the WFR techniques (Trujillo et al., 2011). Deriving a rotor equivalent wind speed model, which accounts for velocity gradients as well as wake characteristics is necessary to improve the accuracy of power and load predictions."

To: "Although the present work does not focus in details on the performance of the two lidar systems, the findings indicate that the main sources of uncertainty in load predictions are related to flow modelling assumptions. The wind velocity gradient in the wake is characterized by the combined effect of the atmospheric shear and the wake deficit. The former can be explained by a power law profile, while the latter is often approximated in the far wake by a Gaussian function, whose depth and width depend on ambient conditions and turbine operation regimes. Further, the 10-min average wind velocity gradient, observed from a fixed point, will be largely influenced by wake meandering in the lateral and vertical directions increasing the complexity of the velocity field in the wake region. The results of the power prediction's deviations in Table 2, in both partial- and full-wake situations, indicate a less accurate reconstruction of the wind field when compared to wake-free conditions. Although we demonstrate a low sensitivity of the loads to the shear exponent for all the analysed sensors (see Fig. 10), it is envisioned to more appropriately account for wake-affected velocity gradient profiles and determine whether or not this will significantly improve the accuracy of power and load predictions"

The following text is added in the conclusion on page 23 line 9:

Future research should apply a wind deficit model that accounts for the combined effect of atmospheric shear and wake deficit, and quantify the uncertainty of resulting power and load predictions.

2. Section 4.3, which presents the validation, is missing structure and components of the validation are not defined. Further, it is not clear to me, why the mast was chosen for the wake-free reference case and not lidar, because this adds another variable in the interpretation.

We conducted an extensive re-structuring of Section 4.3; more details are given in the specific comments below. The mast is here the reference because it would be unfair to choose as reference any of the two lidars. Further, the current IEC load validation approaches under free-wind conditions are based on measurements obtained from a met mast; lidars are still not recommended for load validation purposes. However, following the suggestion of the reviewer, we now use the lidars as the reference case. The load statistics in wake conditions obtained with one of the lidars are compared to the respective statistics of the same lidar in free wind conditions. We keep the results based on the mast for completeness and show the uncertainty of lidar-based load validation in free-wind conditions.

3. The on-board sensor and the simulations are introduced in only one sentence with a reference to another paper. Since they are as integral as the lidars for the validation, they should receive more attention in my opinion.

We added additional details on the on-board sensors in "Sect. 2.2. Measuring campaign" by including the location of the strain gauges on the wind turbine structures (i.e., blades and tower) and the sampling frequency of the load data.

The following text was added on page 4 line 1:

The wind turbine T04 was instrumented with sensors for load measurements at the roots of two blades, tower top, and tower bottom (Vignaroli and Kock, 2016). The strain gauges were installed at 1.5 m from the blade root flange, at 11.85 m below the lower surface of the tower top flange, and at 5.9 m above the upper surface of tower bottom flange. The data acquisition software was set to sample at 35 Hz on all channels. Additional data were provided by the supervisory control and data acquisition (SCADA) system including nacelle wind speed and orientation, power output, blade pitch angles, and generator speed.

We added additional details on the simulations in "Sect. 3 Methodology", including the description of the HAWC2 model and add relative references.

The following text was added on page 6 line 1:

Load simulations are carried out using the state-of-the-art aero-elastic HAWC2 software (Larsen and Hansen, 2007). The structural part of the code is based on a multi-body formulation assembled with linear anisotropic Timoshenko beam elements (Kim et al., 2013). The wind turbine structures (i.e., blades, shaft, tower) are represented by a number of bodies, which are defined as an assembly of Timoshenko beam elements (Larsen et al., 2013).The aerodynamic part of the code is based on the blade element momentum (BEM) theory, extended to handle dynamic inflow and dynamic stall (Hansen et al., 2004), among others. In the present study, the HAWC2 turbine model is based on the structural and aerodynamic data of the Siemens SWT2.3-93 turbine and is equipped with the original equipment manufacturer controller.

References:

Hansen, M., Gaunaa, M., and Aagaard Madsen, H.: A Beddoes-Leishman type dynamic stall model in state-space and indicial formulations, 2004

Kim, T., Hansen, A. M., and Branner, K.: Development of an anisotropic beam finite element for composite wind turbine blades in multibodysystem, Renewable Energy, 59, 172–183, https://doi.org/10.1016/j.renene.2013.03.033, 2013.

I classified this as major revisions, because the first issue could change the results or modify the research questions and conclusions, and the other comments point at an incomplete manuscript. Language: I noticed only a few typos or grammar mistakes in the manuscript with the disclaimer that I am not a native English speaker. Parts of the manuscript would benefit from structuring with subsections and paragraphs (sections 1, 3.4, 4.1, and 4.3 specifically).

Specific comments
- Page 1, line 8-9: This sentence reads to me, that lidar-based load predictions in waked conditions are compared against the mast-based predictions from a mast located in the free wind at the same time. But I believe that the intended meaning is, that the uncertainty of lidar-based predictions against on-board sensors in waked conditions are compared with the uncertainty of mast-based predictions against sensor data in free wind conditions.

The following text was replaced in the abstract on page 1 lines (8-9)

From: "The uncertainty and bias of aero-elastic load predictions are quantified against wind turbine on-board sensor data. We consider mast-based load assessments in free wind as a reference case and assess the uncertainty in lidar-based power and load predictions when the turbine is operating in partial- and full-wake"

To: "We assess the uncertainty of lidar-based load predictions against wind turbine on-board sensors in wake conditions and compare it with the uncertainty of lidar-based load predictions against sensor data in free wind."

- Page 1, line 10: Why is only the smallest increase of the relative error given? What was the largest observed increase?

In order to write a concise and short abstract, we reported the best reachable accuracy of load predictions. However, to show the sensitivity of the error due to inflow wind conditions, we now include the range of the error based on the unfiltered turbulence measures with turbulence length scales as for free wind and waked situations.

The following text is replaced in the the abstract on page 1 lines (10)

From: "Compared to the reference case, the simulations in wake conditions lead to an increase of the relative error as low as 4%"

To: "Compared to the free-wind case, the simulations in wake conditions lead to increased relative errors (4–11%)."

- Page 1, lines 10-11: How do they impact the predictions (e.g. do low wind speed lead to a better uncertainty of the prediction or the opposite?)

The analysis in Fig. 11 shows how uncertainty varies as function of the inflow mean wind speed. The results show that low wind speeds lead to higher bias and uncertainty of the predictions. We also mention it in the text (see Page 20, line 3). This trend is noticeable for power predictions, as the power curve is steeper at low wind speed compared to the curve above rated wind speed (Fig. A.1 in the appendix shows the normalized power curve of the turbine). Further, as the power levels are function of the cube of the wind speed, a small error in the estimated wind speed can lead to a significant bias in the power predictions, particularly at low wind speeds.

The results in Table 2 and 3 show the impact of both turbulence intensity and turbulence length scale on the load predictions. We discuss this impact in "Sect. 4.3 Load simulation results" on page 17 lines 20–32.

We believe that information regarding how the wind field characteristics impact the load predictions and their uncertainty should be found in the related sections in the manuscript. Following the reviewer comment regarding Sect. 4.3, we did an extensive re-structuring of the section, where we clarify the dependency of the uncertainty of predictions on the inflow conditions (see below for more details).

We address the reviewer comment in Sect. 4.4, and we divide the section as into Sect. 4.4 Sensitivity analysis and Sect. 4.4.1 Uncertainty distribution as function of wind speed,

- Fig. 2: The remainder of the manuscript often uses x/D as the upwind distance relative to the turbine with the lidars (opposite to here, where it is the downwind distance from the turbine that causes the wake).

This was corrected. The figure is now replaced by the one below.

- Page 5, eq. (1): Within the wake, the wind speed profile is not following a power law profile.

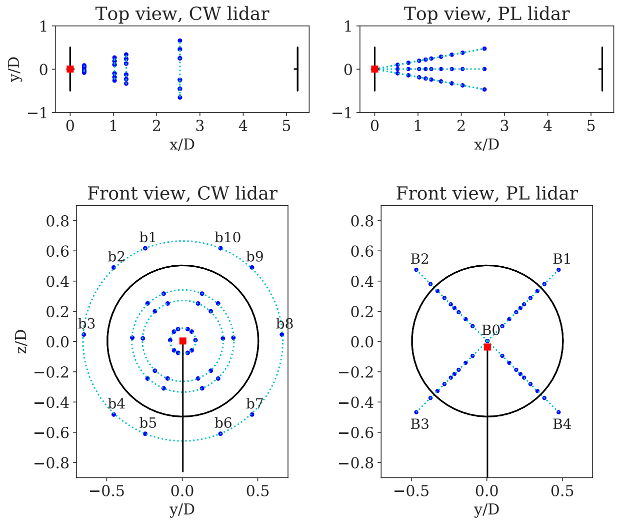

Therefore, I am not convinced that the shear exponent resulting from a partially or fully waked inflow is meaning full. Since the inflow parameters are later used as input for the simulations, the simulated conditions can be expected to be very different from the conditions experienced by the wind turbine. For the CW lidar it seems possible to retrieve spanwise fields of the longitudinal mean velocity provided with some interpolation. Is it possible to initialize the simulations with them instead? As it is, the approach would be better suited to answer what errors are entailed by applying procedures developed for free stream conditions to waked conditions.

Please, see response to major comment nr. 1.

- Page 6, line 2: The simulations should be introduced in more detail.

Please, see response to major comment nr. 3.

- Page 7, line 10: I assume that the assumption of homogeneity is referring to horizontal homogeneity only and not including vertical homogeneity?

The sentence relates to Eq. 5. The inhomogeneities, as wind shear, are introduced after the statement in Eq. 6.

- Fig. 4: Why is the cup anemometer and not the sonic anemometer used for the turbulence measurements? I would expect that the standard deviation from a sonic anemometer is better since it is not affect by cross-contamination and inertia.

The cup is mounted at 80 m, which is the hub height. The sonic is mounted at 76 m. Previous work on the characterization of wind conditions at the NKE site that included wind speed and turbulence showed a discrepancy between the sonic- and cup-based mean wind speed of 2.6% and about 12.3% regarding the longitudinal velocity variance (Peña et al., 2017). To reduce the uncertainty of the mast-based and lidar-based wind characteristics, we choose the cup anemometer for this analysis. The same approach was used in Dimitrov et al. (2019).

The following text is added on page 10, line 8.

Previous work on the characterization of wind conditions at the NKE site that included wind speed and turbulence showed a discrepancy between the 76 m sonic- and 80 m cup-based mean wind speed of 2.6% and about 12.3% regarding the longitudinal velocity variance (Peña et al., 2017). To reduce the uncertainty of the mast-based and lidar-based wind characteristics, we choose the cup anemometer at 80 m, which is the hub height, for this analysis.

- Eq. (14): Why are only the positions B1 and B2 in the upper half of the rotor considered and not the beams B3 and B4 in the lower half?

Preliminary work (Peña et al., 2017) showed that the lidar availability highly reduces when using the bottom beams. This was simply because the lenses of those bottom beams (B3 and B4) became dirty due to contamination from the cleaning system of the CW lidar.

The following text is added on page 11, line 3.

Preliminary work (Peña et al., 2017) showed that the lidar availability highly reduces when using the bottom beams. Therefore, we use the top beams of the PL lidar for this particular analysis.

- Page 12, line 9: How was it determined that the mast is wake-free?

Some details were described on page 11 line 19. However, we now add an Appendix to describe the application of the wake detection algorithm to the mast measurements.

Appendix A: Wake detection from mast measurements

The wake detection algorithm (see Sect.3.4) is extended to the mast measurements to classify 10-min periods where the mast is in free or wake situations. For this purpose, turbulence observations from the cup anemometer at 80 m and vertical wind shear computed using the measurements from the cup anemometers at 57.5 and 80 m are used as wake detection parameters. Their $99th$ percentiles are used as conservative thresholds to characterize the limits of the normal range of the site-specific free wind conditions. The resulting thresholds are $TI_{mast,99} = 0.20$ and $\alpha_{mast,99} = -0.02$. If one of the two limits is exceeded within a 10-min period, the mast is considered in wake conditions and shown with green markers in Fig. 1.

- Fig. 6: As I understood from section 3.1, the effects of the induction zone were removed from the lidar measurements in the wind field reconstruction and the text mentions that the left panel shows reconstructed mean wind speeds (page 12, line 12). Therefore, I am wondering why the effects of the induction zone are present in the lidar data or whether the shown data is based on eq. (5) and not eq. (6)?

We corrected and rephrased the text. In the analysis shown in Fig. 6, we investigate how the lidar-based wind characteristics varies as function of the upstream ranges in free, partial- and full-wake situations. For this particular analysis, we disregard induction effects.

The following text is now added on page 12, line 5:

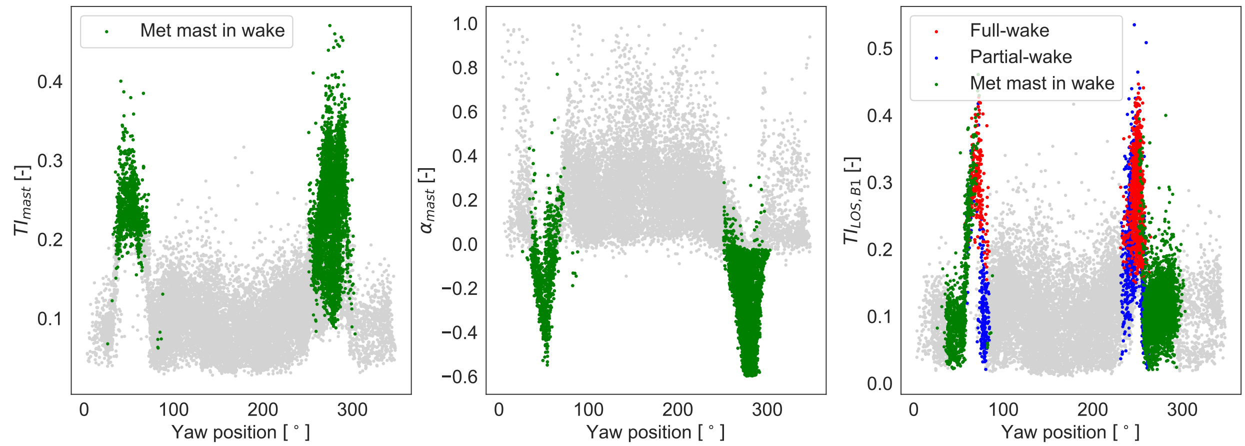

Figure 1: Left and middle: 10-min observations of the turbulence intensity and vertical wind shear at the mast as function of turbine yaw position. Free wind conditions relative to the mast are identified with grey markers, and waked situations with green markers. Right: PL-estimated 10-min wake detection parameter $TI_{LOS,B1}$. Detected wake situations of turbine T04 are shown with coloured markers: wake-free (grey), partial-wake (blue) and full-wake (red). The 10-min periods, where the mast is affected by wakes are shown in green markers.

From: "We observe these effects through the PL and CW lidar-estimated wind speed, turbulence and shear exponent in Fig. 6. Here, the slope of a linear regression model between the free wind mast-measured and lidar-estimated wind parameters in free-, partial- and full-wake situations are shown as function of the upstream distance from the rotor."

To: "Here, the slope (m) of a linear regression model between the free wind mast-measured and lidar-estimated wind parameters in free-, partial- and full-wake situations is shown. In this particular analysis, the lidar-based wind parameters are derived from Eq. (6) evaluated a different upstream distances from the rotor without including induction effects."

- Fig. 6: I am confused, because the axis labels state the ratio between lidar measurements and mast measurements, but the caption states the slope of a linear regression between.

We changed the figure and provided the corrected axis label.

- Page 14, lines 12-14: From the text I understand that for each wind speed bin an ensemble averaged spectrum was computed and to each of those spectra the model is fitted to estimate L (i.e. for each wind speed bin a separate L is computed). However, that does not line up with single spectrum presented in Fig. 7 (left) and three length scales reported in line 24.

This was not correctly described in the manuscript and we replaced the text accordingly. Also, to improve the readability of the manuscript, we divided section 4.1 in: Section 4.1 Wake effects on reconstructed wind parameters and Section 4.2 Wake effects on turbulence spectra properties.

The following text is now replaced in Page 14, lines 12–14:

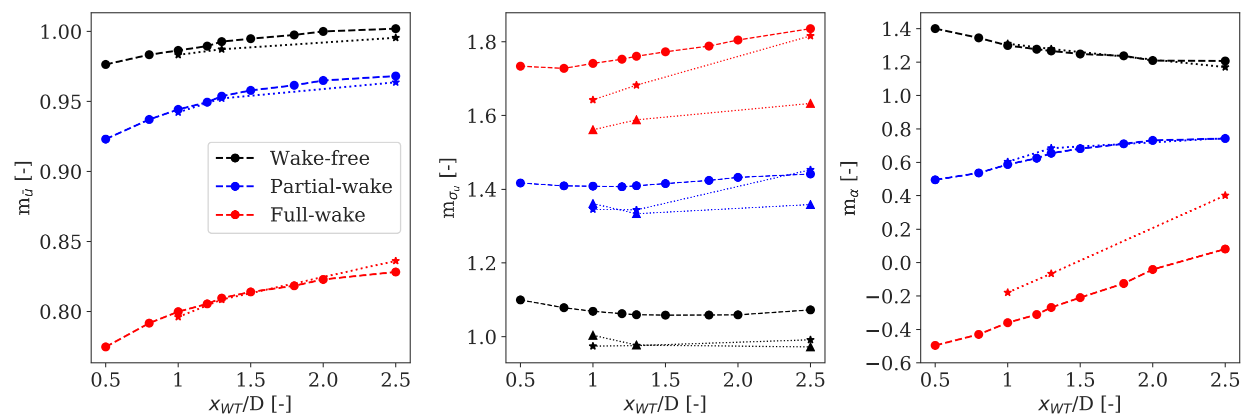

From: "The 10-min time series of radial velocity are classified into wind speed bins and the spectra are ensemble-averaged over each wind speed bin. Then, the parameter L is fitted to the ensemble-averaged spectrum weighted on number of samples in each bin.

To: "The 10-min time series of radial velocity are classified into free-, partial- and full-wake situations and the spectra are ensemble-averaged over all conditions within each class. Then, the parameter L is fitted to the ensemble-averaged spectrum."

- Page 14, lines 17-18: Since the shown spectra are normalized with their respective variance, I don't see this from Fig. 7 (left) and only from Fig. 6 (middle).

The measured and theoretical spectra are normalized over their respective variance under each condition (wake-free, partial wake and full wake). Without normalization, the curves will be all over the place as the energy content under each condition is very different.

- Page 14, line 29: At a given wave number, the turbulence kinetic energy depends on the absolute value of energy spectrum and not its slope. Therefore, I am not understanding this sentence. Also, the term rotor sampling frequency could be explained, because I could not find it in quick search and I am not familiar with it.

We have deleted this sentence as it is confusing. The idea behind this sentence was to explain how the wind field spectra influences the loading conditions on the wind turbine.

- Page 15, line 2: How many bins do you have or what is lowest amount of samples in a bin?

This sentence in the manuscript may mislead the reader, as we do not classify inflow parameters nor simulation results in wind speed bins. Therefore, we have deleted this sentence.

The following text is replaced on Page 15, lines 1-2:

From: "We ensure close to 500 10-min samples, distributed nearly equally among wind speed bins in the range 4–14 m/s, for free-, partial- and full-wake scenarios."

To: "We select around 500 10-min samples for each of the free-, partial- and full-wake scenarios, which are distributed within the wind speed range 4-14 m/s."

- Page 15, line 16 to page 16, line 8: The overall validation approach seems sensible to me. However, in my opinion, it is not clearly written down and has to be pieced together from two different places in the manuscript. Separate subsections for the power and the two bending moment might be help to make it easier to digest. In particular, precise definitions of $\tilde{y}$ and $\hat{y}$ were not provided in this manuscript (I looked at the definitions and explanations in Dimitrov et al. (2019) and hope they are also valid here). Also, the generation of two separate bin averaged wind speed ensemble from the previous section should be recalled here. The difference between the mean and the ensemble average with respect to this data set should be explained explicitly. I believe that an extensive rework of section 3.4 is needed, because I misunderstood an essential part of the validation on my first reading and I believe that was not entirely my own fault.

We now rename section 4.3 from "Load simulation results" to "Load validation procedure" and re-arrange Section 4.3 as:
- Section 4.4 Load validation procedure
- Section 4.4.1 Power predictions
- Section 4.4.2 Extreme load predictions
- Section 4.4.3 Fatigue load predictions

We also rephrase section 4.4 to provide a better description of the validation approach as:

4.4 Load validation procedure
The load validation analysis is conducted on the dataset described in Sect. 4.3. We analyze about 500 10-min samples distributed between 4-–14 m/s, for free-, partial- and full-wake scenarios. The quality of load predictions is evaluated through one-to-one comparisons against load measurements. The resulting statistics from HAWC2 simulations are denoted by ($\tilde{y}$) and the corresponding measured statistics from the turbine on-board sensors by ($\hat{y}$). Three uncertainty-related indicators are assessed, where the symbol $E(.)$ denotes the mean value and $\langle . \rangle$ the ensemble average.

- Coefficient of determination $R^2 = \langle(\tilde{y} - E(\tilde{y}))^2\rangle / \langle(\hat{y} - E(\hat{y}))^2\rangle$
- Uncertainty $X_R = \sqrt{\langle(\tilde{y}/\hat{y} - E(\tilde{y})/E(\hat{y}))^2\rangle}$
- Bias $\Delta_R = E(\tilde{y})/E(\hat{y})$

The R^2, X_R, Δ_R indicators are computed for free-, partial- and full-wake situations. The 10-min wind turbine statistics investigated hereafter include the mean power production ($\mathrm{Power}_{\mathrm{mean}}$), the extreme loads and 1-Hz damage equivalent fatigue loads of fore-aft tower bottom bending moment ($\mathrm{M_{xTB_{max}}}, \mathrm{M_{xTB_{DEL}}}$) and flapwise bending moment at the blade root ($\mathrm{M_{xBC_{min}}}, \mathrm{M_{xBC_{DEL}}}$). Therefore, time-series of 600 s are simulated in the aero-elastic code HAWC2 and load statistics are derived at the location where the strain gauges are installed. A turbulence seed with statistical properties matching those of the measured 10-min conditions is input to the load simulations. The rainflow counting algorithm is used to compute the 1-Hz damage equivalent fatigue loads with Whöler exponent of $m = 12$ for blades and $m = 4$ for the tower. The same approach is used to post-process measured loads. We run simulations using wind field characteristics listed in Table 1, which are derived from both the PL and CW lidars as well as the mast measurements. A more detailed analysis is conducted for partial- and full-wake situations. Here, we investigate how power and load predictions are influenced by filtered and unfiltered turbulence estimates derived in Sect. 4.3, characteristic turbulence length scales derived in Sect. 4.4 and wind parameters derived from lidar measurements at several ranges. We provide detailed scatter plots of measured and predicted load sensors used in the analysis in Figs. B1-B5 in the Appendix. The predictions uncertainties for power production and extreme loads are presented in Table 2, and for fatigue loads in Table 3. We define the lidar-based power and load predictions in free wind as the reference case. Thus, we compare the relative error between the uncertainty indicators derived from wake situations with those from the free wind case. Generally, we observe lower prediction accuracy in partial- and full-wake situations compared to the free wind scenario, while in some cases similar uncertainty levels are obtained. The following sections describe the results in details.

4.4.1 Power predictions

Power production levels are overestimated in partial-wake, but underestimated in full-wake by approximately 4% compared to the free wind case. Larger X_R values are found in full-wake compared to the reference case, although R^2 is above 96%, which indicates a good correlation. We do not observe a significant influence of turbulence intensity levels on power predictions, i.e. by comparing the uncertainties in full-wake between simulations performed with filtered and unfiltered turbulence estimates from the CW lidar in Table 2. In a similar way, small turbulence length scales derived in wakes have a negligible effect on power production levels. The power predictions deviations in partial-wake drop to approximately 1%, when the PL lidar-estimated wind characteristics using measurements up to 1.3 D are used in the simulations. This result indicates the sensitivity of the reconstructed wind field characteristics to the upstream ranges in a strongly inhomogeneous wind field as a partial-wake situation.

4.4.2 Extreme load predictions

The extreme loads ($\mathrm{M_{xTB_{max}}}, \mathrm{M_{xBC_{min}}}$) are both affected by the turbulence levels as well as the turbulence length scale. We obtain similar deviations in partial- and full-wake as per the free wind conditions, when using unfiltered turbulence estimates and length scales extracted in free wind conditions (see Table 2). However, simulations based on filtered turbulence consistently overestimate extreme load levels (3–7%). The effect of a low value for the length scale is noticeable in full-wake situations, where $L = 7$ m leads to biases of the order of -7% compared to the reference case. Overall, higher X_R values are derived in wakes compared to the reference, while R^2 remains above 89% in all analyzed cases. It should also be noticed that the maximum loads do not increase significantly in wake situations, since the wind speed in the wakes is lower than the free wind (Larsen et al., 2013).

4.4.3 Fatigue load predictions

The biases of fatigue load predictions in partial-wake, using unfiltered turbulence statistics and $L = 35$ m, are comparable with the deviations observed in free wind conditions, as seen in Table 3. The error increases when filtered turbulence from the PL lidar are simulated, leading to an underestimation of fatigue loads between 2–5%. The most significant deviations are observed for $\mathrm{M_{xTB_{DEL}}}$ and $\mathrm{M_{xBC_{DEL}}}$ in full-wake conditions. The simulations based on filtered turbulence measures and $L = 35$ m lead to an overestimation of blade-root and tower-bottom predictions by 21% compared to the free wind case. The filtered turbulence statistics are predicted with the use of the spectral velocity tensor model and are found to be approximately 11% higher compared to unfiltered turbulence derived from the Doppler radial velocity spectrum (see Fig. 9-middle). The bias

of fatigue load predictions drop to approximately 11%, when unfiltered turbulence measures from the CW lidar are simulated. Overall, extreme and fatigue load predictions show low uncertainty when unfiltered turbulence estimates are used as input in simulations.
Fatigue loads are found to correlate significantly better when a synthetic turbulent field characterized by small length scales is used (i.e. $L = 7$ m). This is demonstrated by improved X_R and R^2 indicators compared to those resulting from simulations with $L = 35$ m. Besides, reducing L from 35 m (free-wind conditions) to 7 m (fitted in full-wake conditions) reduces fatigue blade-root load levels by 15%. The simulations with low length scales and unfiltered turbulence measures provide the lowest deviations in full-wake compared to the reference case, as the error drops to -4% for $\mathrm{M_{xBC_{DEL}}}$, indicating underprediction (see Table 3). These results demonstrate the improved accuracy of load predictions when unfiltered turbulence measures are simulated, and validate the importance of characterizing turbulence spectral parameters for load analysis; as previously demonstrated in Thomsen and Sørensen (1998), Sathe et al. (2012), and Dimitrov et al. (2017).

- Page 15, line 18: Check equation. The square should be outside of the bracket.

This is now corrected.

- Page 15, line 19: Check equation. Missing a square.

This is now corrected.

- Page 17, line 8: I am not yet understanding why this bias ratio was chosen as an indicator for the behavior of the uncertainty. With a mast-based reference case, there are two influencing factors with (1) the differences between mast vs. lidar and (2) waked vs. free wind conditions. Why not use lidar-based predictions for free wind conditions as the reference? Then only waked vs. free wind conditions remain, which would make interpretation easier.

Following the suggestion of the reviewer, we changed the reference case, so it is now the lidar-based load predictions in free wind conditions.

Also, in later occurrences of the bias ratio it is not stated whether it is an over- or underestimation (I am assuming that both 1.02 and 0.98 would be given as 2%).

We added the signs to differentiate over- and under-estimation and also specified whether is under- or over-prediction.

- Page 17, line 20: The section is already quite loaded. It might be worth to consider to separate the filtered and unfiltered comparison from the rest of the section. The same might be considered for the length scale.

By re-structuring Section 4.3 into four subsections, as described above, Sect. 4.4.3 Fatigue load predictions will be easier to read.

- Page 18, lines 11: I believe it should be “the increased effect”.

This is now corrected.

- Page 18, lines 12: I believe it should be “higher”.

The first entry “high” describes the fact that we measure high turbulence levels in the wake; the second entry “higher” work as a comparative, in this case between the turbulence levels under wake- and free conditions.

- Page 18, line 15: Why is the effect of L in the sensitivity analysis minor, but it had an effect of up to 15% in the previous section (Table 2)?

The results in Fig. 10 should be interpreted as the coefficients of a linear regression model between the inputs and the output sensors. The regression models are fitted to a dataset of 850 10-min periods, which are characterized by different inflow conditions (i.e. wind speed, turbulence, shear, etc.) as measured by the PL lidar and the L parameter, which was varied between the defined boundaries (see figure below for the partial-wake). Note that we show the absolute input values in the figure, although the inputs are normalized such that their values are scaled between zero and one, when fitting the regression model. The resulting coefficients give an estimation of the slope of a linear model between inputs and outputs. If a strong dependency is seen between output and inputs, as for the mean wind speed and turbulence in the figure below, a strong sensitivity of output sensor to the input is indicated. In the case of L, we do not see a linear relationship, but rather a scatter plot. This is because, while we vary L, the wind speed and turbulence levels are also varied, and the impact of the latter two is higher to that of L. However, when all inputs are fixed and only L varies, as the results in Table 2 and Table 3, we can estimate the effective influence of L on the predictions.

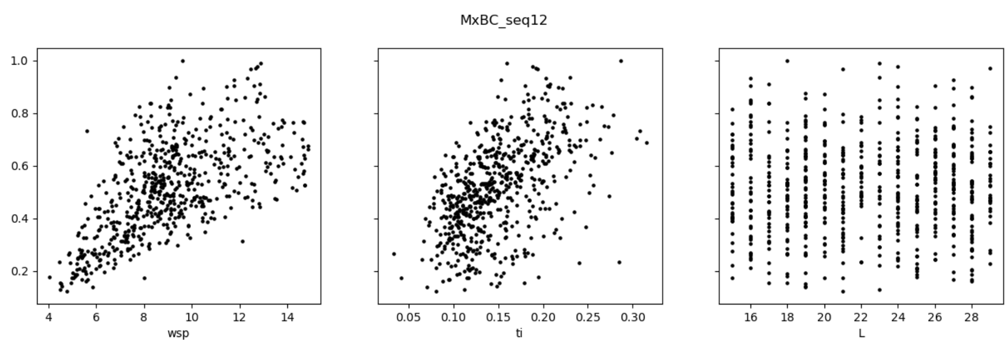

Figure 2: Scatter plot of the normalized fatigue loads at the blade-root as function of inflow wind conditions (mean wsp, turbulence and turbuelence length scale L)

- Page 22, lines 10-11: Consider rephrasing this sentence, because it can be understood in two ways.

The sentence “The effective turbulence approach under predicted fatigue load levels at spacings larger than 5 D (Schmidt et al., 2011).” is now deleted, in case this is what the reviewer was pointing at

- Page 22, lines 27-28: Reiterating a previous comment, I am not convinced that the power law should be applied within the wake, because the wind profile has a different shape. The conclusion regarding the vertical wind profile here is based on the sensitivity to the shear exponent and I am not convinced that it holds for the same reason, because the simulated wind fields might have been very different from the real wind field. Also, I am confused regarding the horizontal wind profile, because I cannot remember that horizontal gradients were accounted for in the wind field retrieval. Is that referring to the wind veer maybe?

Please, see the response to major comment nr. 1. We deleted the sentence regarding the horizontal gradient and now discuss the influence of turbulence intensity and turbulence length scale on the power productions levels, as shown below.

The following text is replaced on Page 22, lines 27-28:

From: “Power production levels under wake conditions were strongly related to the mean wind speed at hub height, whereas the vertical and horizontal wind profiles had negligible effects on those levels”

To: “Power production levels under wake conditions were strongly driven by the reconstructed wind speed at hub height, whereas turbulence intensity as well as turbulence length scales had negligible effects on those levels.”

- Page 29, lines 23-24: The reference of Dimitrov et al. (2019) seems to be out of place and should appear after Dimitrov et al. (2018) assuming the sorting hierarchy is first author alphabetical followed by year.

This is now corrected.

Aero-elastic load validation in wake conditions using nacelle-mounted lidar measurements

Davide Conti[1], Nikolay Dimitrov[1], and Alfredo Peña[1]

[1]Department of Wind Energy, Technical University of Denmark, Frederiksborgvej 399, 4000 Roskilde, Denmark

Correspondence: Davide Conti (davcon@dtu.dk)

Abstract. We propose a method for carrying out wind turbine load validation in wake conditions using measurements from forward-looking nacelle lidars. Two lidars, a pulsed and a continuous wave system, were installed on the nacelle of a 2.3 MW wind turbine operating in free-, partial- and full-wake conditions. The turbine is placed within a straight row of turbines with a spacing of 5.2 rotor diameters and wake disturbances are present for two opposite wind direction sectors. ~~We account for wake-induced effects by means of wind field parameters~~ The wake flow fields are described by lidar-estimated wind field characteristics, which are commonly used as inputs for load simulations, ~~which are reconstructed using lidar measurements~~without employing wake deficit models. These include mean wind speed, turbulence intensity, vertical and horizontal shear, yaw error and turbulence-spectra parameters. ~~The uncertainty and bias of aero-elastic load predictions are quantified~~ We assess the uncertainty of lidar-based load predictions against wind turbine on-board ~~sensor data. We consider mast-based load assessments in free wind as a reference case and assess the uncertainty in~~ sensors in wake conditions and compare it with the uncertainty of lidar-based ~~power and load predictions when the turbine is operating in partial- and full-wake~~load predictions against sensor data in free wind. Compared to the ~~reference~~ free-wind case, the simulations in wake conditions lead to ~~an increase of the relative error as low as~~ increased relative errors (4~~%~~–11%). It is demonstrated that the mean wind speed, turbulence intensity and turbulence length scale have a significant impact on the predictions. Finally, the experiences from this study indicate that characterizing turbulence inside the wake as well as defining a ~~rotor equivalent wind speed~~ wind deficit model are the most challenging aspects of lidar-based load validation in wake conditions.

1 Introduction

Wind turbines are designed according to reference wind conditions described in the IEC standards (IEC, 2019). These reference conditions are used to establish the full design load basis and for the purpose of certification of turbine designs. Nevertheless, certified turbines need to be further verified that they can withstand the site-specific loads during the entire lifetime, when site-conditions exceed those of the type-certified. As a current best practice, the wind turbine (WT) operating loads are predicted using high-fidelity aero-elastic simulations based on site-specific environmental conditions. The environmental conditions are typically obtained from anemometers installed on meteorological masts in the proximity of the wind turbine location. These mast measurements, and therefore the uncertainty quantification of the aero-elastic model, are usually limited to wake free sectors. However, wind conditions inside wind farms are significantly different than those in undisturbed wind conditions (Frandsen, 2007). Wake effects are responsible for wind speed reduction and turbulence levels increase, generally resulting in reduced power productions and increased load levels (Larsen et al., 2013). To account for these effects, aero-elastic load simulations are combined with wake models, which predict wake-induced effects on the flow field approaching individual WTs. The most applied approach consists of increasing the turbulence in load simulations, resulting in a load increase which should correspond to the effect of the wake-added turbulence. The effective turbulence depends on the park layout and on the material properties of the turbine components under consideration (Frandsen, 2007). This approach is recommended by the IEC 61400-1. An alternative and more detailed practice also described in the IEC standard relies on the use of the Dynamic Wake Meandering (DWM) model (Larsen et al., 2006, 2007; Madsen et al., 2010), which is an engineering model providing simulated wind field time series including wake deficits. The comparison of fatigue loads predicted using the DWM model and the effective turbulence approach by the IEC showed a discrepancy of 20% (Thomsen et al., 2007). The uncertainty varied according to the inflow conditions and spacing between turbines. The work of Larsen et al. (2013) showed a very fine agreement between both power and load measurements and predictions based on a site-specific calibrated DWM model for the Dutch Egmond aan Zee wind farm. However, the study did not quantify uncertainty in a systematic approach. More recently, Reinwardt et al. (2018) estimated fatigue load biases in the range 11–15% for the tower bottom and 8–21% for the blade-root flapwise bending moments using the DWM model. To date, these approaches are characterized by a significant level of uncertainty, due to the stochastic nature of environmental conditions and the various simplifying assumptions used in the wake model definitions ~~(Schmidt et al., 2011; Reinwardt et al., 2018).~~ (Schmidt et al., 2011). Further, these results motivate the need for improving wind turbine load validation approaches in wake conditions.

The recent applications of lidars in the wind energy field demonstrate the feasibility of these systems to reconstruct inflow wind conditions including mean wind speed (Raach et al., 2014; Borraccino et al., 2017), turbulence ~~(Mann et al., 2009; Branlard et al., 2013; Peñ~~ (Mann et al., 2009; Branlard et al., 2013; Peña et al., 2017; Newman and Clifton, 2017) and wake characteristics ~~(Bingöl et al., 2010; Mac~~ (Bingöl et al., 2010; Iungo and Porté-Agel, 2014; Machefaux et al., 2016), among others. Nacelle-mounted lidars enable us to measure wind field characteristics for any wind direction/nacelle yaw position, including situations when the turbine rotor is in the wake of a neighbouring turbine. An excellent level of agreement has been found between the nacelle-mounted lidar-estimated and mast-measured mean wind speed in free wind conditions (Borraccino et al., 2017). Power curve validations using nacelle-mounted lidars have been showing promising results (Wagner et al., 2014). Although lidar-derived along-wind variances could deviate from those derived from cup anemometer measurements (Peña et al., 2017), the load predictions in wake-free sectors based on nacelle-lidar wind field representations resulted in uncertainties lower than or equal to those obtained with mast measurements (Dimitrov et al., 2019). Based on these findings, we extend the load validation procedure defined in Dimitrov et al. (2019) to include wake conditions. Therefore, wake-induced effects are accounted for by means of wind field parameters commonly used as inputs for load simulations, which are reconstructed using lidar measurements, yet without employing wake deficit models. The objective of this study is to demonstrate how loads in wake conditions can be predicted accurately, quantify the uncertainty, and compare it to the uncertainty of ~~mast-based~~ lidar-based load assessments in free wind. The further development of lidar-based load and power validation procedures can potentially replace the use of expensive meteorological masts in measurement campaigns as well as improve the wake field reconstruction for aero-elastic load simulations.

The paper is structured as follows. In Sect. 2, we introduce the requirements for load validation and describe the measurement campaign. In Sect. 3, we present the methods implemented to derive the wind field parameters for aero-elastic simulations and a wake detection algorithm. The results are provided in Sect. 4. First, we show the wake-induced effects on the lidar-estimated wind field parameters in ~~Sect. 4.1~~ Sects. 4.1 and 4.2. Then, we derive the wind field characteristics used as input for load simulations in Sect. 4.3. The uncertainties of load predictions are quantified in Sect. 4.4~~and a sensitivity analysis to assess the influence~~. The sensitivity of inflow parameters on load predictions ~~is carried out~~ and the uncertainty distribution of selected cases are assessed in Sect. 4.5. Finally, we discuss the findings and provide conclusions in the last two sections.

2 Problem formulation

2.1 Requirements for load validation in wakes

The design load cases and load validation procedure for wind turbines are described in the IEC standards. The IEC61400-1 requires the evaluation of fatigue and extreme loading conditions induced by wake effects originating from neighboring wind turbines. The increase in loading due to wake effects can be accounted for by the use of an added turbulence model, or by using more detailed wake models (i.e., DWM). Load validation guidelines are described in IEC61400-13 (IEC, 2015), which recommends the so-called one-to-one comparison, among few approaches. This approach consists of carrying out individual aeroelastic simulations for each measured realization of environmental conditions. To date, wind conditions are obtained from meteorological masts. The objective of this work is to carry out load validation of wind turbines operating in wake conditions using measurements from nacelle-mounted lidars only. The wake-induced effects are accounted for by lidar-estimated wind field characteristics, without employing wake deficit models. This implies that wake flow fields can be described by means of average flow characteristics commonly used as inputs for load simulations. We assess the viability of the suggested approach by carrying out a load validation study as following:

- One-to-one load comparison between measured and predicted load realizations using wind field characteristics derived from lidar measurements of the wake flow field.
- Uncertainty quantification in terms of the statistical properties of the ratios between measured and predicted load realizations.
- Comparison of lidar-based load predictions uncertainties in wakes against uncertainties of load predictions in free wind conditions using ~~mast~~ lidar measurements.

We assume that the observed deviations in load predictions between those that are lidar-based under wake conditions and those that are ~~mast-based~~ lidar-based under free wind conditions are solely due to the error in the wind field representation. This is a simplistic but conservative assumption, as the uncertainties of load predictions are a combination of uncertainty in the reconstructed wind profiles, aero-elastic model uncertainty, load measurement uncertainty as well as statistical uncertainty (Dimitrov et al., 2019).

2.2 ~~Measuring~~ Measurement campaign

Wind and load measurements are collected from an experiment conducted at the Nørrekær Enge (NKE) wind farm during a period of 7 months between 2015 and 2016. The farm is located in the North-west of Denmark and consists of 13 Siemens 2.3 MW turbines, with a 93-m rotor diameter (D) and hub height of 80 m above ground level. The turbines are installed in a single row oriented along the 75° and 255° direction compared to true north, with 487-m (5.2 D) spacing, as pictured in Fig. 1. The wind farm is located over flat terrain and the surface is characterized by a mix between croplands and grasslands, and a fjord to the north (Peña et al., 2017). The prevailing wind direction is west (Borraccino et al., 2017). The wind turbine T04 was instrumented with sensors for load measurements at the roots of two blades, tower top and tower bottom (Vignaroli and Kock, 2016). The strain gauges were installed at 1.5 m from the blade root flange, at 11.85 m below the lower surface of the tower top flange, and at 5.9 m above the upper surface of tower bottom flange. The data acquisition software was set to sample at 35 Hz on all channels. Additional data were provided by the supervisory control and data acquisition (SCADA) system including nacelle wind speed and orientation, power output, blade pitch angles, and generator speed. A meteorological mast was installed at 232 m (2.5 D) distance from T04 in direction 103°. The mast instrumentation comprises cup and sonic anemometers, wind vanes and thermometers mounted at several heights, among others. Details about the instrumentations can be found in Vignaroli and Kock (2016) and Borraccino et al. (2017). This study uses wind measurements from the cup anemometers at 57.5 and 80 m, which are used to derive wind speed, turbulence and shear as discussed in the following sections. According to the definition in IEC61400-12-1 (IEC, 2017), the wake-free sector spans approximately 123°, from 97° to 220°. A narrow sector of 12° span from 97° to 109° is chosen as free wind reference to ensure close correspondence between lidar- and mast-measured parameters. Based on the farm geometry and visual inspection of data, wake sectors of 30° are considered ranging from 55° to 85° for north-east directions and from 235° to 265° for south-west.

2.3 Lidars

Two forward-looking lidars were installed on the nacelle of T04: a pulsed lidar (PL) with a 5-beam configuration and a continuous wave (CW) system. The CW lidar by ZephIR has a single beam, which scans conically with a cone angle of 15° and a sampling frequency of 48.8 Hz. The CW lidar measured sequentially at five different ranges upwind from the turbine, at 0.1, 0.3, 1.0, 1.3 and 2.5 D, and took approximately 50 s to complete a full scan at all ranges. The CW lidar measurements are binned according to the azimuthal positions in 50 bins of 7.2°. Based on Dimitrov et al. (2019), we select 10 of these bins for further analysis and focus on ranges between 0.3 and 2.5 D, as illustrated in Fig. 2 (bottom-left). The PL lidar provided by Avent technology has five fixed beams; a central beam oriented in the longitudinal direction at hub height and four beams

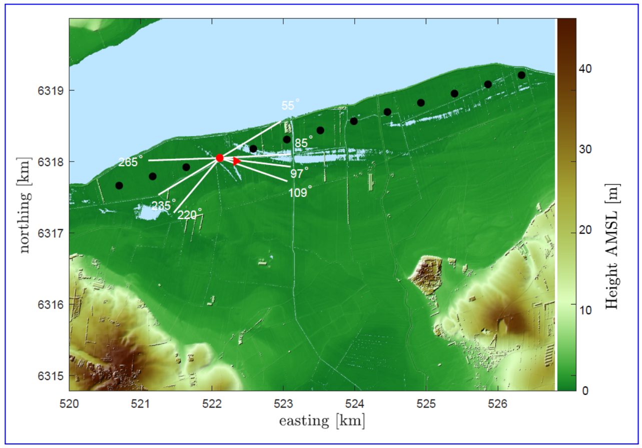

Figure 1. The Nørrekær Enge wind farm in northern Denmark on a digital surface elevation model (UTM32 WGS84). The wind turbines are shown in circles, the turbine T04 with the nacelle lidars in red and the mast in a triangle. The sectors used for the analysis are also shown; narrow direction sector: 97°– 109°; wide direction sector: 97°– 220°; wake sectors: 55°– 85° and 235°– 265°. The waters of Limfjorden are shown in light blue.

oriented at the corner of a square pattern, as shown in Fig. 2 (bottom-right). The PL lidar measures simultaneously at ten different ranges in front of the turbine 0.53, 0.77, 1.03, 1.17, 1.30, 1.53, 1.78, 2.03, 2.5, and 3.0 D, by acquiring radial velocity spectra for 1 s at each beam, thus scanning a single plane with a sampling frequency of 0.2 Hz (Peña et al., 2017). To provide a direct comparison with results from the CW lidar, we focus the analysis on the PL lidar measurements up to 2.5 D. More details of the lidars are described in Peña et al. (2017) and Dimitrov et al. (2019), while calibration reports are provided in Borraccino and Courtney (2016a, b). The top views of the PL scanning pattern and CW lidar binned data selection are illustrated in Fig. 2 (top). The lidars measure approximately within 2.5 and 5 D downstream of the wake-source turbine. We conduct the load analysis using 10-min reference periods. The dataset is filtered so that we select only periods where the turbine is operational and load, mast and lidar measurements are available. A total of 6198 10-min periods are available in the wide direction sector, which reduces to 1042 samples in the narrow sector. The majority of measurements within the wake sectors are from westerly directions 235°– 265° with 3659 samples, while 899 samples are available from wake directions 55°– 85°.

3 Methodology

Load simulations are carried out using the state-of-the-art aero-elastic HAWC2 software (Larsen and Hansen, 2007). The structural part of the code is based on a multi-body formulation assembled with linear anisotropic Timoshenko beam elements (Kim et al., 2013). The wind turbine structures (i.e. blades, shaft, tower) are represented by a number of bodies, which are defined as an assembly of Timoshenko beam elements (Larsen et al., 2013). The aerodynamic part of the code is based on the blade element momentum (BEM) theory, extended to handle dynamic inflow and dynamic stall (Hansen et al., 2004), among others. In the present study, the HAWC2 turbine model is based on the structural and aerodynamic data of the Siemens SWT

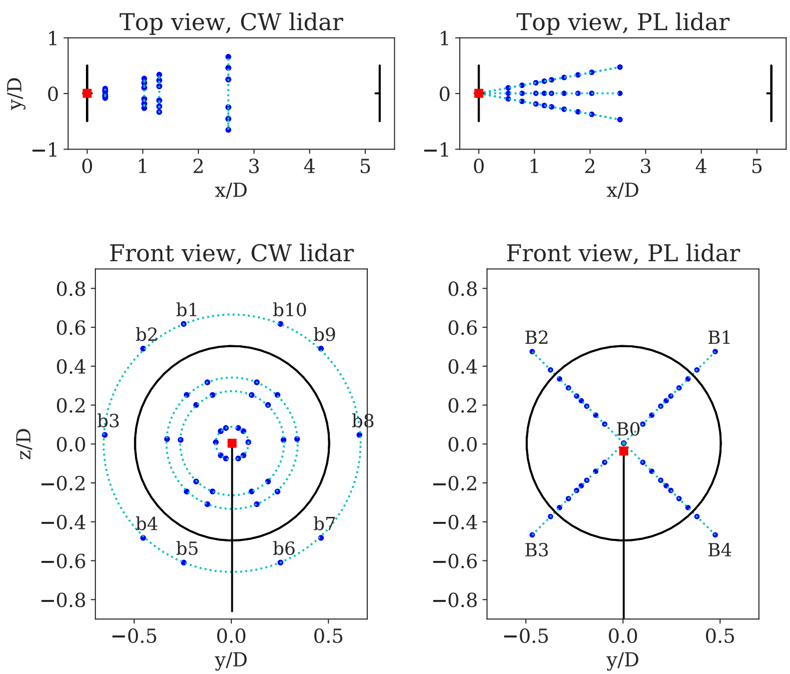

Figure 2. Top and front views of the CW lidar (left) and PL lidar (right) scanning patterns shown by the blue dots. The trajectory of the lidars beams is illustrated by the dotted lines in cyan. The bins/beams notation is also given. The location of the lidars on T04 is shown with a red square marker. The reference coordinate system has an origin at the hub center with the x-axis is in the mean wind direction. The distances are normalized with respect to the rotor diameter D.

2.3-93 turbine and is equipped with the original equipment manufacturer controller. The turbulence used in the simulations is generated using the Mann turbulence model ~~(Mann, 1994)~~(Mann, 1994, 1998). As described in Dimitrov et al. (2018), the turbulent wind field for aero-elastic simulations can be fully characterized statistically by nine environmental parameters listed in Table 1. The methods to derive the wind field parameters from the radial velocity measurements of the nacelle-mounted lidars are described in Sects. 3.1–3.3. We propose a wake detection algorithm to detect wakes using lidar measurements in Sect. 3.4.

Table 1. Wind field parameters serving as input for aeroelastic load simulations.

Description	Parameter	Description	Parameter
Mean wind speed at hub height	$\bar{u}_{hub}$	Air density	ρ
Turbulence intensity	$\cancel{\sigma_U/U}$ $\sigma_u/\bar{u}$	Mann turbulence spectra tensor parameters:	
Shear exponent	α	turbulence length scale	L
Wind veer	$\Delta\varphi$	anisotropy factor	Γ
Yaw misalignment	$\bar{\varphi}$	turbulence dissipation parameter	$\alpha_k\epsilon^{2/3}$

3.1 Wind field reconstruction

Wind field reconstruction (WFR) is defined as the process of retrieving wind field characteristics by combining measurements of the wind in multiple locations (Raach et al., 2014; Borraccino et al., 2017). As nacelle-mounted lidars measure only the line-of-sight (LOS) component of the wind vector, WFR techniques are used to derive the input wind field variables for carrying out load simulations. The present work implements the WFR technique described in Dimitrov et al. (2019). This approach assumes three-dimensional wind vectors, vertical and horizontal wind profiles combined with an induction model. The vertical wind shear is defined by a power law profile,

$$\bar{u}(z) = \bar{u}_{hub} \left(\frac{z}{z_{hub}} \right)^{\alpha}, \tag{1}$$

where z_{hub} is the hub height. The flow direction $\varphi(z)$ is described by the combined effects of the mean yaw misalignment and the change of wind direction with height, the wind veer,

$$\varphi(z) = \bar{\varphi} + \frac{\Delta\varphi}{D}(z - z_{hub}). \tag{2}$$

We assume a linear variation of wind direction over the rotor diameter D. To define the relation between the free-flow wind vector $\boldsymbol{u} = (u, v, w)$ and the LOS velocity u_{LOS}, we consider a reference coordinate system with origin at hub height and co-linear with the wind turbine orientation. The wind coordinate system is aligned with the mean wind direction, which is defined by the flow direction in Eq. (2). Thus, the transformation from the wind- into the reference-coordinate system is achieved by the rotational transformation $\boldsymbol{T_1}$:

$$\boldsymbol{T_1} = \begin{bmatrix} \cos\varphi(z) & -\sin\varphi(z) & 0 \\ \sin\varphi(z) & \cos\varphi(z) & 0 \\ 0 & 0 & 1 \end{bmatrix}. \tag{3}$$

Note that the wind flow inclination (tilt) is neglected. The orientation of the LOS velocity with respect to the reference coordinate system is defined by rotations about the y- and z-axes, ψ_y and ψ_z ~~.~~ (see Fig. A1 in the Appendix). Therefore, the transformation from the LOS- into the reference-coordinate system is achieved by the rotational transformation $\boldsymbol{T_{LOS}}$:

$$\boldsymbol{T_{LOS}} = \begin{bmatrix} \cos\psi_y \cos\psi_z & -\cos\psi_y \sin\psi_z & \sin\psi_y \\ \sin\psi_z & \cos\psi_z & 0 \\ -\sin\psi_y \cos\psi_z & \sin\psi_y \sin\psi_z & \cos\psi_y \end{bmatrix}. \tag{4}$$

~~Eventually, the~~ As lidars measure only the LOS velocity, the first row alone of T_{LOS} is considered. The relation between the wind vector and the LOS velocity is expressed in terms of matrix transformations as:

$$\boldsymbol{u_{los}} = \boldsymbol{T_{LOS}} \boldsymbol{T_1} \boldsymbol{u}. \tag{5}$$

This formulation is suitable assuming lidar point-like measurements and homogeneous wind field, which implies that the three velocity component statistics do not change over the scanned area. ~~As lidars measure only the LOS velocity component, the first row alone of $\boldsymbol{T_{LOS}}$ is considered.~~ By combining Eqs. (1)-(5) and including an induction factor C_{ind} based on a two-dimensional induction model (Dimitrov et al., 2019), the relation between the LOS and the wind velocity field is derived in its extended form as:

$$u_{LOS} = \\ = \bar{u}_{hub}\left(\frac{z_1}{z_{hub}}\right)^{\alpha}\left[C_{ind}\cos\left(\bar{\varphi}+\frac{\Delta\varphi}{D}(z-z_{hub})\right)\cos\psi_y\cos\psi_z - \sin\left(\bar{\varphi}+\frac{\Delta\varphi}{D}(z-z_{hub})\right)\cos\psi_y\sin\psi_z\right]. \quad (6)$$

~~The parameters $(\bar{u}_{hub},\alpha,\Delta\varphi,\bar{\varphi})$~~

The two-dimensional induction model assumes longitudinal and radial variation of the induced wind velocity. The resulting induction factor C_{ind} is computed as:

$$C_{ind} = \left[1 - a_0\left(1-\frac{\xi_x}{\sqrt{1+\xi_x^2}}\right)\cdot\left(\frac{2}{\exp(+\beta_a\epsilon_a)+\exp(-\beta_a\epsilon_a)}\right)^2\right], \quad (7)$$

where a_0 is the induction factor at the rotor center area; $\xi_x = x/R_{rotor}$ is the distance from the rotor normalized by the rotor radius; $\rho_a = \sqrt{y^2+z^2}/R_{rotor}$ is the radial distance from the rotor center axis; $\epsilon_a = \rho_a/\sqrt{\lambda_a(\eta_a+\xi_x^2)}$, where $\gamma_a = 1.1$, $\beta_a = \sqrt{2}$, $\alpha_a = 8/9$, $\lambda_a = 0.587$, $\eta_a = 1.32$ (Dimitrov et al., 2019). The parameters $(\bar{u}_{hub},\alpha,\Delta\varphi,\bar{\varphi},C_{ind})$ from Eq. (6) are to be characterized by the WFR, while x,y,z describe the spatial location of the measurement points. The WFR approach relies on a model-fitting technique and consists in minimizing the residual between the modelled wind field and lidar measurements (Borraccino et al., 2017). The CW and PL lidar-estimated mean wind speed in free wind, for the narrow direction sector (97°–109°), are compared with measurements from the 80 m cup anemometer mounted on the mast in Fig. 3 (left and middle). An excellent agreement is found for the lidar-estimated mean wind speed using both lidars. The lidar-estimated shear exponents are compared with the shear obtained by fitting the power law profile using measurements from the cups at 57.5 m and 80 m in Fig. 3 (right). The observed deviations result from the use of different parts of the rotor span by the PL lidar compared to the mast measurements (Dimitrov et al., 2019). Besides, the shear exponents derived by the CW lidar compare very well with those from the PL lidar (not shown).

3.2 Turbulence spectral model

The wind field vector $\boldsymbol{u}(\boldsymbol{x})$ can be described by the solely spatial vector $\boldsymbol{x} = (x,y,z)$, assuming Taylor's frozen turbulence hypothesis (Mizuno and Panofsky, 1975). The ~~velocity fluctuations~~statistics of velocity fluctuations (u',v',w'), where $(')$ denotes fluctuations around the mean value, ~~denoted by $\boldsymbol{u} = (u,v,w)$,~~ are expected homogeneous in space (Mann, 1994). It follows that the auto- or cross-covariance function between two points can be defined only in terms of the separation distance as $R_{ij}(\boldsymbol{r}) = \boldsymbol{u}_i'(\boldsymbol{x})\boldsymbol{u}_j'(\boldsymbol{x}+\boldsymbol{r})\rangle$, where i, j = (1,2,3) are the indices corresponding to the components of the wind field, $\langle\rangle$ denotes

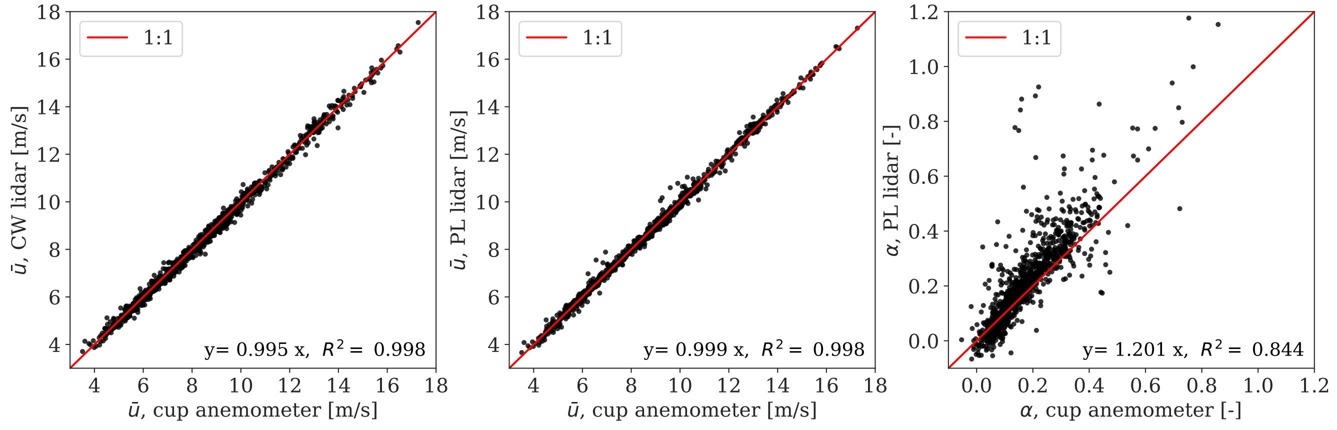

Figure 3. Comparison of 10-min lidar-estimated and mast-measured inflow characteristics. We show a 1:1 line for guidance, the slope of a linear regression model and the coefficient of determination R^2.

ensemble averaging, and $\boldsymbol{r} = (r_1, r_2, r_3)$ is the separation vector in the three-dimensional Cartesian coordinate system. The covariance tensor of single-point turbulent statistics $(\boldsymbol{R}(\boldsymbol{r}=0) = \boldsymbol{R})$ can be written as:

$$\boldsymbol{R} = \begin{bmatrix} \langle u'u' \rangle & \langle u'v' \rangle & \langle u'w' \rangle \\ \langle v'u' \rangle & \langle v'v' \rangle & \langle v'w' \rangle \\ \langle w'u' \rangle & \langle w'v' \rangle & \langle w'w' \rangle \end{bmatrix} \approx \begin{bmatrix} \sigma_u^2 & \sigma_{uv} & \sigma_{uw} \\ \sigma_{vu} & \sigma_v^2 & \sigma_{vw} \\ \sigma_{wu} & \sigma_{wv} & \sigma_w^2 \end{bmatrix}, \tag{8}$$

where the matrix elements define variances and covariances of the three-dimensional velocity field $\boldsymbol{u} = (u, v, w)$. The spectral velocity tensor $\Phi_{ij}(\boldsymbol{k})$ is defined as the Fourier transform of the covariance tensor,

$$\Phi_{ij}(\boldsymbol{k}) = \frac{1}{(2\pi)^3} \int R_{ij}(\boldsymbol{r}) \exp(i\boldsymbol{k} \cdot \boldsymbol{r}) d\boldsymbol{r}, \tag{9}$$

where ~~$\boldsymbol{r} = (r_1, r_2, r_3)$ is the separation vector in the three-dimensional Cartesian coordinate system and~~ $\boldsymbol{k} = (k_1, k_2, k_3)$ is the wave number vector. The spectral velocity tensor can be described by the model of Mann (1994). This model requires only three parameters: $\alpha_k \epsilon^{2/3}, L$ and Γ, where α_k is the spectral Kolmogorov constant, ϵ is the turbulent energy dissipation rate, L is a length scale proportional to the size of turbulence eddies, and Γ is a parameter describing the anisotropy of the turbulence. Although the Mann model assumes near-neutral atmospheric conditions, the model has been applied to different surface and atmospheric-stability conditions (Peña et al., 2010). The one-point spectra are computed as:

$$F_{ij}(k_1) = \int \int \Phi_{ij}(\boldsymbol{k}, \Gamma, L, \alpha_k \epsilon^{2/3}) dk_2 dk_3. \tag{10}$$

The procedure to derive spectral parameters from the measured spectra of the three velocity components is described in Mann (1994). The LOS spectra measured by a lidar beam can be related to the velocity spectral tensor by accounting for probe volume effects as described in Mann et al. (2009),

$$F_{LOS}(k_1) = n_i n_j \int\int |\, \hat{\phi}(\boldsymbol{k}\cdot\boldsymbol{n})\,|^2\, \Phi_{ij}(\boldsymbol{k},\Gamma,L,\alpha_k\epsilon^{2/3})dk_2dk_3, \tag{11}$$

where $\hat{\phi}$ is the Fourier transform of the lidar spatial weighting function and $\boldsymbol{n}$ is the unity vector along the beam. For a CW lidar, this is typically described by a Lorentzian function (Sonneschein and Horrigan, 1971; Mann et al., 2010). For the pulsed lidar, we assume a Gaussian weighting function (Frehlich, 2013).

3.3 Turbulence characterization

Turbulence characterization using lidars is subjected to several sources of uncertainty. The measurement volumes along the LOS lead to spatial averaging of turbulence, which reduces the LOS variance when compared to a point measurement (Sjöholm et al., 2008; Sathe and Mann, 2013). Besides, the ability to properly measure the variances of the velocity components depends on the scanning strategy. Since the lidar beams are rarely aligned with any of the three velocity components, the LOS variance can be influenced by the variance of other velocity components, also referred to as cross-contamination effects. We implement two approaches to derive filtered and unfiltered turbulence based on the work of Peña et al. (2017). The first approach uses the turbulence spectral model by Mann to correct turbulence estimates by accounting for the expected attenuation of the fluctuations of the radial velocity due to the lidar's probe volume. This can be achieved numerically by deriving the relation between the variance of the LOS velocity with and without filtering effects, respectively $\sigma^2_{u,LOS,va}$ and $\sigma^2_{u,LOS,pt}$. The filtering is expressed by:

$$r(Z_r,L,\Gamma,\psi_y,\psi_z)^2 = \frac{\int_0^\infty F_{LOS}(k_1)dk_1}{\int_0^\infty F_{ij}(k_1)dk_1} = \frac{\sigma^2_{u,LOS,va}}{\sigma^2_{u,LOS,pt}}. \tag{12}$$

The magnitude of r^2 varies in relation to the probe volume length Z_r, turbulence characteristics and spatial location of measurement points (Mann et al., 2010; Peña et al., 2017). Following the procedure described in Dimitrov et al. (2019), the covariance matrix of the filtered LOS velocity components $\boldsymbol{R_{LOS}}$ can be related to the covariance of the undisturbed wind field $\boldsymbol{R}$. To express the LOS variance as function of the u-component variance, we normalize $\boldsymbol{R}$ with respect to $\cancel{\sigma^2_U}\sigma^2_u$. We neglect the terms σ^2_{uv} and σ^2_{vw} as they are small and we lack sufficient information to recover all components. Hence, we derive the ratios between variances of different velocity components using the spectral tensor model by Mann (1994),

$$\frac{\boldsymbol{R}}{\sigma^2_u} = \begin{bmatrix} 1 & 0 & \sigma_{uw}/\sigma^2_u \\ 0 & \sigma^2_v/\sigma^2_u & 0 \\ \sigma_{wu}/\sigma^2_u & 0 & \sigma^2_w/\sigma^2_u \end{bmatrix}. \tag{13}$$

The effects of cross-contamination and flow direction are accounted for by means of matrix transformations including $\boldsymbol{T_{LOS}}$ and $\boldsymbol{T_1}$. The relation between the covariance matrix of the LOS components and that of the undisturbed wind field is then expressed in terms of $\cancel{\sigma^2_U}\sigma^2_u$ as:

$$\frac{\boldsymbol{R_{LOS}}}{\sigma^2_u} = r(Z_r,L,\Gamma,\psi_y,\psi_z)^2 \left(\boldsymbol{T_{LOS}CT_1}\frac{\boldsymbol{R}}{\sigma^2_u}\boldsymbol{T_1^T C^T T_{LOS}^T}\right), \tag{14}$$

where $\boldsymbol{C}$ is the induction matrix (Dimitrov et al., 2019). ~~Since~~ Note that $\boldsymbol{R_{LOS}}$ is expressed as a full covariance matrix containing three vector components. However, as only LOS velocities are measured by the nacelle-mounted lidar, ~~the~~ only the first component of $\boldsymbol{R_{LOS}}$ is measured. It follows that the ratio in Eq. (14) identifies the relation between the LOS variance and the wind field variance in the longitudinal direction. Eventually, the variance of the wind field is computed by scaling the variance of the LOS residuals with the reciprocal of the filtering ratio estimated using Eq. (14). The procedure is described in details in Dimitrov et al. (2019). The second approach avoids filtering effects by use of the ensemble-averaged Doppler radial velocity spectrum (Mann et al., 2010). This method relies on the hypothesis that the lidar average Doppler spectrum is related to the probability density function of the radial velocities (Branlard et al., 2013). This assumption is valid for homogeneous flow and for negligible velocity gradients within the probe volume. By assuming homogeneous ~~wind flow~~turbulence, we use the scanning pattern to account for cross-contamination of different velocity components and ~~we~~ extract 10-min σ_u^2 statistics by computing the variance of Eq. (5) ~~. We refer the reader to~~ as:

$$\mathrm{Var}(u_{los}) = \mathrm{Var}\left((\cos\psi_y \cos\psi_z \cos\varphi - \cos\psi_y \sin\psi_z \sin\varphi)u - (\cos\psi_y \cos\psi_z \sin\varphi + \cos\psi_y \sin\psi_z \cos\varphi)v + (\sin\varphi)w\right). \quad (15)$$

By solving the variance operator and neglecting the resulting terms $\langle u'v' \rangle$ and $\langle v'w' \rangle$, as explained above, σ_u^2 is derived as shown in Eq. (10) in Peña et al. (2017)~~for the extended expression.~~

. We show the comparison between lidar-estimated and mast-measured σ_u, using the ~~80 m~~ 80 m cup anemometer, for free wind and narrow direction sector (97°– 109°) in Fig. 4. Previous work on the characterization of wind conditions at the NKE site that included wind speed and turbulence showed a discrepancy between the 76 m sonic- and 80 m cup-based mean wind speed of 2.6% and about 12.3% regarding the longitudinal velocity variance (Peña et al., 2017). To reduce the uncertainty of the mast-based and lidar-based wind characteristics, we choose the cup anemometer at 80 m, which is the hub height, for this analysis. The filtered turbulence derived from CW and PL lidars, using all the ranges and beams, are plotted respectively in Fig. 4 (left and middle), whereas the unfiltered turbulence derived from the CW lidar measurements at 1.3 D are shown in Fig. 4 (right). The deviations between PL lidar and the cup anemometer values are mostly due to high-frequency noise contamination as described in Peña et al. (2017). Considering the wind conditions within the free wind narrow direction sector, the lidar-estimated turbulence compares very well with mast measurements; the observed results are consistent with previous findings (Dimitrov et al., 2019).

3.4 Wake detection algorithm

A wake detection algorithm is developed to determine whether the turbine is operating in free-, partial- and full-wake situations. The algorithm relies on 10-min statistics of the lidar measurements and follows the approach of Held and Mann (2019). The idea is to detect the increase in turbulence originating from wakes with respect to the free wind conditions. This can be done by measuring turbulence intensity TI_{LOS} and the relative turbulence difference measured by two lidar beams pointing at two opposite rotor sides, δTI_{LOS}. The detection parameters are:

$$TI_{LOS} = \frac{\sigma_{LOS}}{u_{LOS}}, \qquad \delta TI_{LOS} = \frac{TI_{LOS,B1} - TI_{LOS,B2}}{\langle TI_{LOS,B1}, TI_{LOS,B2} \rangle}, \quad (16)$$

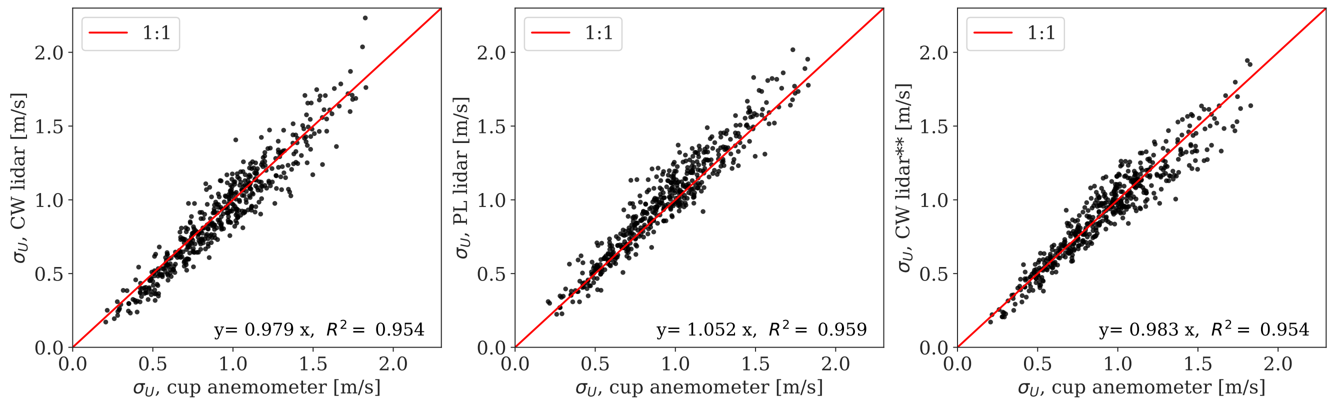

Figure 4. Left and middle: comparison of the lidar-based σ_U, derived with the use of the spectral tensor model, with σ_U values measured with 80-m cup anemometer mounted on the mast. Right: comparison of lidar-based σ_U, derived from the ensemble-averaged Doppler spectrum of the CW lidar, with σ_U values measured with 80-m cup anemometer. We show a 1:1 line for guidance, the slope of a linear regression model and the coefficient of determination R^2.

where $B1$ and $B2$ refer to the PL lidar beam notation given in Fig. 2. Preliminary work (Peña et al., 2017) showed that the lidar availability highly reduces when using the bottom beams. Therefore, we use the top beams of the PL lidar for this particular analysis. Due to its location (see Fig. 1), the mast is either in the wake of T04 for wind directions coming from south-west or in the wake of the upstream turbines for north-east directions. As a consequence, we cannot rely on mast measurements to monitor free wind conditions for wind directions within our range of interest. Therefore, we propose an alternative approach, which relies on lidar measurements only. At first, we fit the wake detection parameters to a probability distribution function (pdf) using data from the wake-free wide direction sector (97°– 220°). We select a log-normal and normal pdf for TI_{LOS} and δTI_{LOS}, and choose the $99th$ percentile as conservative thresholds characterizing the limit of the normal range of the site-specific free wind conditions. This results in $TI_{LOS,99} = 0.276$ and $\delta TI_{LOS,99} = 0.416$. Hence, we compare the detection parameters in wake sectors to the precomputed thresholds and classify accordingly. The parameters are shown as function of the turbine yaw positions and classified as partial-wake (blue markers) and full-wake (red markers) in Fig. 5 (left and middle). A partial-wake situation is detected for $\delta TI_{LOS} > \delta TI_{LOS,99}$, whereas the sign of δTI_{LOS} indicates which half of the rotor is affected by the wake. A full-wake is detected when both beams exhibit high turbulence $TI_{LOS,B1,B2} > TI_{LOS,99}$, but $\delta TI_{LOS} < \delta TI_{LOS,99}$. This condition appears when both beams are measuring inside the wake. Figure 5 (right) illustrates the measured fatigue blade root flapwise bending moments for wind speeds between 8 and 10 m/s, as function of the turbine orientation. Fatigue load levels are normalized with respect to the average value computed using load measurements from the free wind wide direction sector. The 10-min periods in which the turbine is operating in wake situations are shown based on the detection algorithm. A significant wake-induced effect on the load levels can be noticed. Further, we attempt to distinguish situations where the mast is in wake or in free wind, based on 10-min mast data. Turbulence from the cup at 80 m and shear derived from the cups at 57.5 m and 80 m are used as wake detection parameters (results are ~~not shown~~ shown in Fig. B1 in the Appendix). The wake detection results presented in Fig. 5 are obtained using the PL lidar-estimated filtered turbulence at 1.3 D. An in-depth comparison between the PL and CW lidars, filtered and unfiltered turbulence estimates and measurements at several ranges are omitted in the present work. Improved wake detection can be obtained by establishing thresholds conditional to the ambient wind conditions (i.e., wind speed, turbulence and atmospheric stability) and by assessing the detection parameters for shorter time periods (Held and Mann, 2019). More detailed detection algorithms including wake dynamic characteristics are proposed in the literature (Aitken and Lundquist, 2014; Aitken et al., 2014). Nevertheless, the proposed algorithm is able to detect 10-min periods where dominant wake effects are observed. The conservative thresholds ensure a strong wake influence in the inflow conditions and a sufficient number of 10-min periods are obtained for the purpose of load validation.

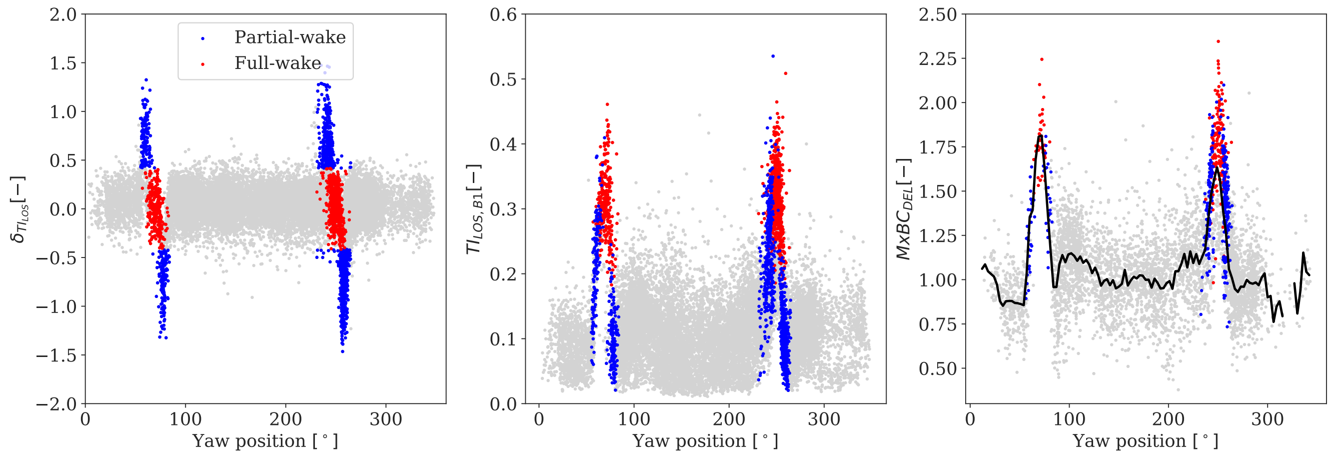

Figure 5. Left and middle: PL lidar-estimated 10-min wake detection parameters δTI_{LOS} and $TI_{LOS,B1}$, as function of yaw position. Detected wake situations are shown with coloured markers: wake-free (grey), partial-wake (blue) and full-wake (red). Right: measured blade-root flapwise fatigue loads for wind speeds between 8 and 10 m/s, normalized over the average load levels in free wind conditions. The black line shows the average values binned every 3° directions.

4 Results

The results are presented in ~~four~~ five parts. The wake-induced effects on the reconstructed wind field parameters are analyzed in ~~Sect. 4.1~~ Sects. 4.1 and 4.2. The wind field parameters used as input for aero-elastic simulations are derived in Sect. 4.3. The one-to-one load comparison between simulated and measured loads and their uncertainty quantification are presented in Sect. 4.4. In Sect. 4.5, we assess the sensitivity of inflow parameters on load predictions and investigate the uncertainty distribution as function of the wind speed.

4.1 Wake effects on reconstructed wind parameters

Wind turbine wakes lead to a region characterized by reduced wind speed and increased turbulence. We observe these effects through the PL and CW lidar-estimated wind speed, turbulence and shear exponent in Fig. 6. Here, the slope (m) of a linear regression model between the free wind mast-measured and lidar-estimated wind parameters in free-, partial- and full-wake situations ~~are shownas function of the upstream distance~~ is shown. In this particular analysis, the lidar-based wind parameters are derived from Eq. (6) evaluated a different upstream distances from the rotor without including induction effects. The 10-min periods are classified according to the results of the wake detection algorithm in Sect. 3.4, considering south-westerly directions (235°– 265°). There are 287 and 175 periods respectively, where partial- and full-wake situations are detected, while the mast is wake-free. The wake-free mean wind speeds range between 4–14 m/s at turbulence levels between 5–15%. Although wake effects vary according to the ambient wind field, we select all measured conditions for this comparison. The influence of wakes on the lidar-estimated mean wind speed is shown in Fig. 6 (left). The reconstructed velocities in partial-wake (blue markers) and full-wake (red markers) are respectively ∼5% and ∼20% lower than ambient wind speed. The magnitude of the velocity deficit depends on the number and location of lidar beams that are measuring inside the wake. Figure 6 (left) also shows the influence of rotor induction at shorter ranges, where low velocity is measured in the vicinity of the turbine (Mann et al., 2018). Despite that velocity recovery is expected moving downstream the wake, the induction effects are predominant. Altogether the PL and CW lidar-estimated mean wind speeds differ from each other by less than 2% in the analyzed cases. We compare lidar-measured σ_u levels inside the wake against σ_u measured by the mast in free wind in Fig. 6 (middle). The bias of PL lidar filtered turbulence (circle markers) and the CW lidar filtered and unfiltered (star and triangle markers) are shown as function of upfront rotor distance. The results show clearly the increased turbulence in partial- and full-wake. The ~~inter-comparison~~ difference between PL and CW filtered turbulence in wake situations ~~shows low bias~~ (circle and star markers) decreases at farther beams, where larger probe volume averaging effects are expected for the CW lidar (Dimitrov et al., 2019). The main discrepancy is found for filtered and unfiltered turbulence estimates in wake conditions, where the latter are significantly lower. We do not observe significant induction effects on the estimated σ_u, as they affect to a much lower extent the velocity variance (Simley et al., 2016; Mann et al., 2018). A slight wake recovery can be also noticed, specifically in full-wake situations (red markers), where lower σ_u are estimated moving downstream. The estimated shear exponent through the PL and CW lidar for free and wake conditions is shown in Fig.6 (right). As wakes expand both horizontally and vertically, wake effects can be related to a decrease of the shear exponent compared to free wind flow and even negative values in full wake. The differences between the PL and CW lidar-estimated shear are most pronounced in full wake, where the CW measures at multiple points in the vertical direction. The fitted shear can also be used as an indicator of wake influence on inflow measurements.

4.2 Wake effects on turbulence spectral properties

In addition to the wake-induced effects on the average flow properties, turbulence spectral properties are also affected in wake regions. Earlier work on this subject showed a shift of the wake spectrum towards low length scales, compared to the free wind spectrum, both in wind tunnel and field experiments (Vermeer et al., 2003). Although large variations in length scales occurred

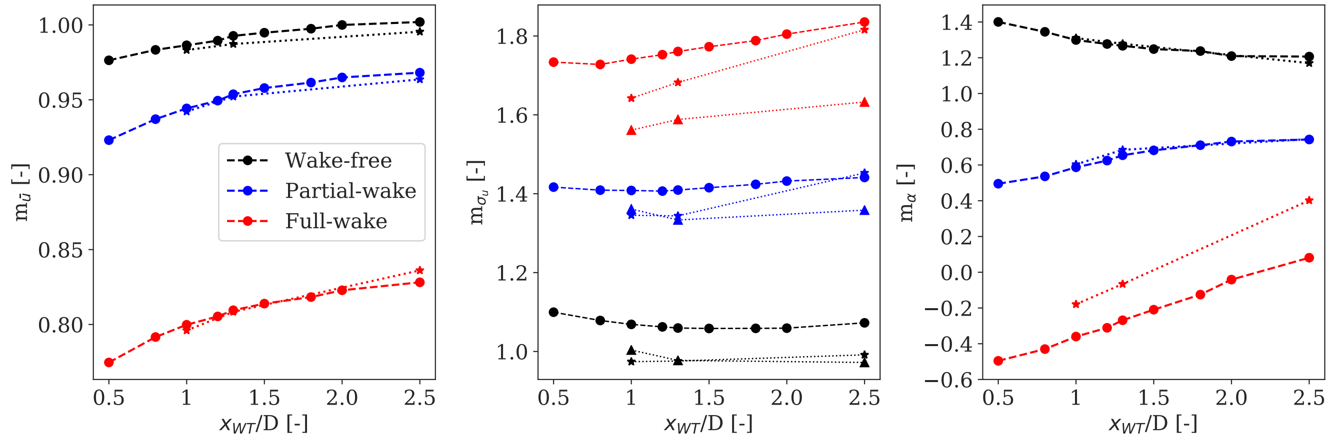

Figure 6. Comparison of the slope of a linear regression model between lidar-estimated and mast-measured inflow characteristics including mean wind speed (left), the standard deviation of wind speed (middle) and shear (right), when the turbine is operating in wake-free (black), partial-wake (blue) and full-wake (red) conditions and the met mast measures free wind conditions. Results are shown as function of lidar measuring distances upfront the rotor and normalized over rotor diameter. The results for the PL lidar are shown by the dash-line with circle markers, whereas those for the CW lidar by the dotted line with star markers. The triangle markers shows unfiltered turbulence obtained from the ensemble-average Doppler spectrum of the CW lidar.

due to atmospheric stability, it was generally observed that wake induced turbulence is characterized by a significantly smaller length scale than that for ambient turbulence (Chamorro et al., 2012). Furthermore, wake-added turbulence can be modelled using synthetic turbulence field with a small length scale, as done for the DWM model (Larsen et al., 2008). Based on these findings, we extract the turbulence spectra parameters of the Mann model, with focus on the length scale L, in free-, partial- and full-wake situations. By comparing lidar spectra to spectra from sonic anemometer in wake-free conditions at NKE, it was found that lidar measurements can qualitatively represent turbulence spectra, although differences increase for turbulence length scales comparable to the probe volume length (Peña et al., 2017; Dimitrov et al., 2019). We ensemble-average lidar radial velocity spectra using the central beam $(B0)$ of the PL lidar. Assuming that the turbine is aligned with the inflow wind direction, the central beam pointing upstream at hub height is ideally measuring the wind fluctuations of the horizontal velocity component. In this case, minimal contamination effects from other velocity components are expected. Typically, three auto-spectra of the wind velocity components as well as one-point cross-spectrum are fitted simultaneously to the theoretical spectra to derive the Mann-model parameters. However, as we measure a single LOS spectrum, we assume $\Gamma = 3$, which is suitable for the terrain and climate for free-wake conditions (Peña et al., 2017). Although Γ impacts load predictions, the influence of the turbulence length scale was found to be predominant (Dimitrov et al., 2017, 2018). The 10-min time series of radial velocity are classified into ~~wind speed bins and~~ free-, partial- and full-wake situations and the spectra are ensemble-averaged over ~~each wind speed bin~~all conditions within each class. Then, the parameter L is fitted to the ensemble-averaged spectrum~~weighted on number of samples in each bin~~. The comparison is based on the energy spectra of the u-velocity component (along-wind) in free-, partial- and full-wake situations. The measured and theoretical spectra, normalized over ~~σ_u^2~~the relative variance, are shown in Fig. 7 (left). The aggregated measured spectra in wakes show a shift of spectrum peak towards higher wave numbers, as expected, which indicates high energy content at low turbulence length scales. ~~Besides, increased level of variance is observed in both partial- and full-wake compared to the values in free wind conditions.~~ The deviations between the modelled and the measured spectra increase ~~for~~ under wake situations. This follows from the limitations of the Mann model, which was developed for homogeneous wind flow and near-neutral atmospheric conditions, the constraints of the adopted fitting procedure and due to the uncertainty of the lidar-measured spectra. In fact, the derived length scale values are critically affected by the probe volume filtering effects, atmospheric stability conditions, sampling frequency and measurements location in the wake region. Resulting length scales of approximately 35, 15 and 7 m are estimated, respectively, for free-, partial- and full-wake conditions. These values are used to generate synthetic turbulence fields for load simulations. The ~~observed magnitude of decrease in longitudinal turbulence length scale is larger than a factor of two as found in Frandsen (1996), but consistent with results reported in Thomsen and Sørensen (1998) and Madsen et al. (2010), where wake-added turbulence is characterized by length scales within the range 10–25% of the free-wind length scale. In addition, we observe a steeper slope of the wake spectra towards higher wavenumbers, which reduces the turbulence energy content within the range of rotor sampling frequencies. Small-scale turbulence is also responsible for increasing the width of the Doppler spectrum~~ small-scale turbulence generated within wake flows generally leads to a significantly larger broadening of the Doppler spectrum compared to that in the ambient flow (Branlard et al., 2013; Held and Mann, 2019). We show an example of a 10-min ensemble-average Doppler spectrum obtained from the radial velocity of the CW lidar using bins *b3* and *b8* (see Fig. 2 for notation) at 1.3 D in partial-wake and full-wake in Fig. 7 (middle and right). ~~The relative free wind speed measured at the met mast is 9 m/s~~We also provide the ensemble-average Doppler spectrum in free wind for reference. It can be noticed that broadening effects are present only in *b3* (solid blue line) in the partial-wake and in both bins (solid and dashed red lines) in full-wake conditions.

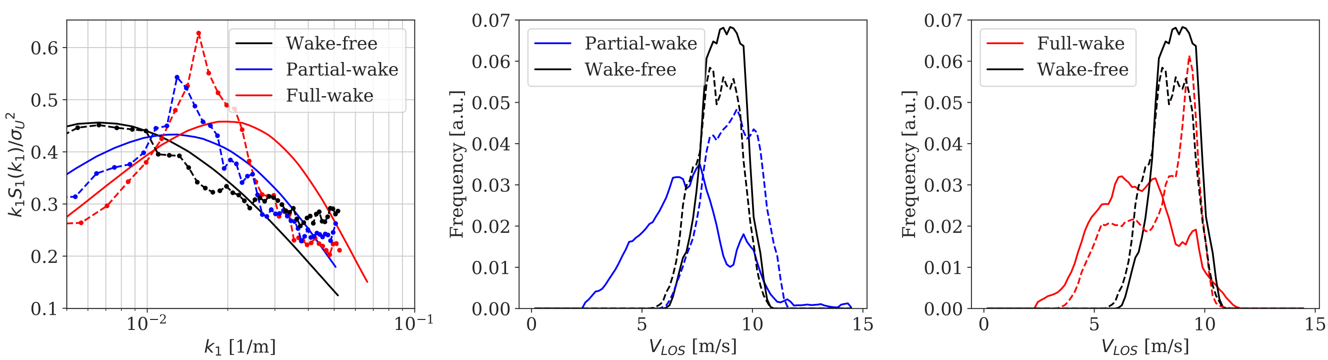

Figure 7. Left: comparison of the normalized ensemble-average u_{LOS}-spectrum based on measurements with the central beam of the PL lidar (dash-line and markers) against the fitted theoretical Mann spectra using Eq. (11) (solid line). Middle and right: normalized ensemble-average Doppler spectrum measured over a 10-min period by the CW lidar using bins *b3* (solid line) and *b8* (dash line).

4.3 Reconstructed inflow parameters for load simulations in wake situations

~~We ensure close to~~ We select around 500 10-min samples ~~, distributed nearly equally among wind speed bins in the range 4–14 m/s, for free-,~~ for each of the free-, partial- and full-wake ~~scenarios~~scenarios, which are distributed within the wind speed range 4-–14 m/s. We select 10-min periods within the narrow sector (97°– 109°) for free flow conditions and periods of south-west directions (235°– 265°) for wake situations. The main limitation of the current dataset is given by the concurrent availability of both lidars and by the few 10-min periods at high wind speeds in full-wake situations. The comparison of the reconstructed wind field characteristics in partial-wake conditions using PL and CW lidar measurements from all ranges is presented in Fig. 8. A very good agreement can be observed for the mean wind speed; the line fits yield slopes of nearly unity and an R^2 of almost 100%. The filtered turbulences from the PL lidar are $\sim$ 2% lower than those from the CW lidar. The differences can be partly explained by the larger amount of filtering occurring for farther beams of the CW lidar as well as due to the distinct scanning patterns measuring an inhomogenous wind flow. When compared to the filtered turbulence, the unfiltered estimations show a significant reduction by $\sim$ 6% (blue markers in Fig. 8 middle). A large scatter appears for the shear, veer and yaw (the latter two are not shown), which are subjected to a high level of uncertainty and highly depend on the scanning patterns. Similar results are found for full-wake situation as presented in Fig. 9. The main discrepancy is in the estimation of the shear exponent.

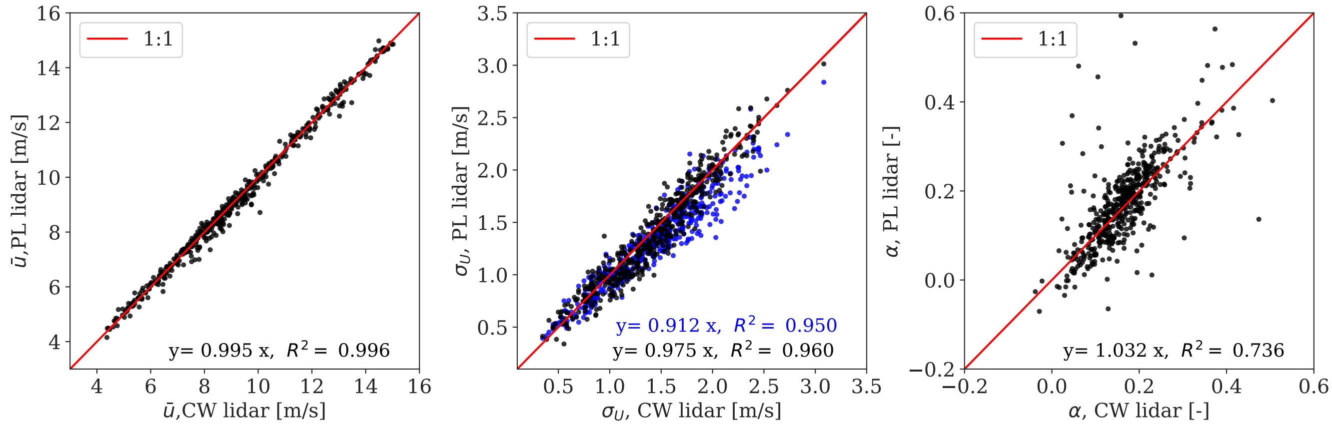

Figure 8. Comparison of the CW and PL lidar 10-min reconstructed wind speed (left), filtered and unfiltered turbulence in black and blue color, respectively, (middle), and shear exponent (right) for partial-wake conditions. We show a 1:1 line for guidance, the slope of a linear regression model and the coefficient of determination R^2.

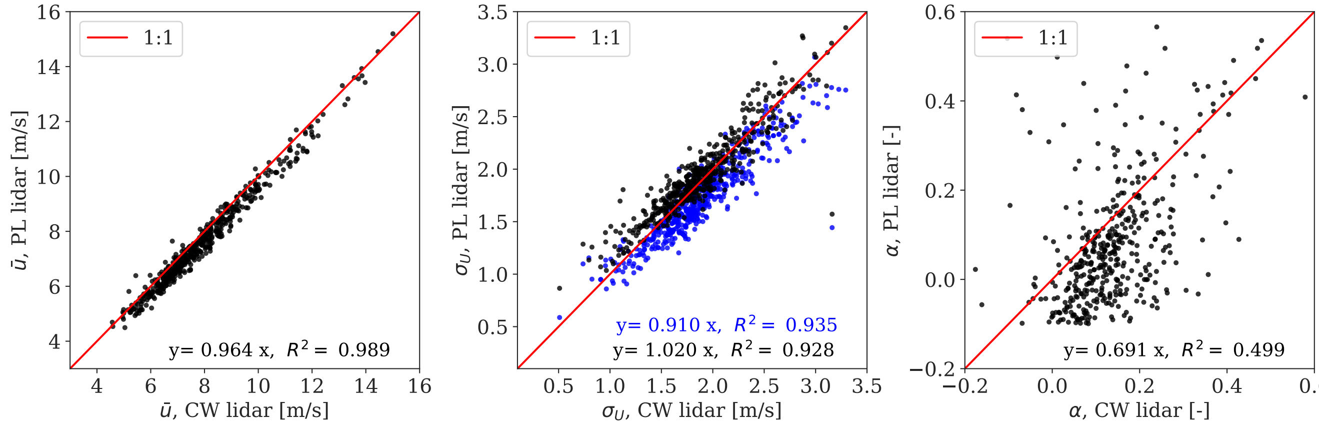

Figure 9. Same as Fig. 8 but for full-wake conditions

4.4 Load ~~simulation results~~validation procedure

The load validation analysis is conducted on the dataset described in Sect. 4.3. We analyze about 500 10-min samples distributed between 4–-14 m/s, for free-, partial- and full-wake scenarios. The quality of load predictions ~~($\tilde{y}$)~~ is evaluated through one-to-one ~~comparison~~ comparisons against load measurements~~(~~. The resulting statistics from HAWC2 simulations are denoted by ($\tilde{y}$) and the corresponding measured statistics from the turbine on-board sensors by ($\hat{y}$). Three uncertainty-related indicators are assessed, where the symbol $E(.)$ denotes the mean value and $\langle . \rangle$ the ensemble average.

- Coefficient of determination ~~$R^2 = \langle(\tilde{y} - E(\tilde{y})^2)\rangle / \langle(\hat{y} - E(\hat{y})^2)\rangle$~~ $R^2 = \langle(\tilde{y} - E(\tilde{y}))^2\rangle / \langle(\hat{y} - E(\hat{y}))^2\rangle$
- Uncertainty ~~$X_R = \sqrt{\langle(\tilde{y}/\hat{y}) - E(\tilde{y})/E(\hat{y})\rangle}$~~ $X_R = \sqrt{\langle(\tilde{y}/\hat{y} - E(\tilde{y})/E(\hat{y}))^2\rangle}$
- Bias $\Delta_R = E(\tilde{y})/E(\hat{y})$

The R^2, X_R, Δ_R indicators are computed for free-, partial- and full-wake situations. The 10-min wind turbine statistics investigated hereafter include the mean power production ($\mathrm{Power_{mean}}$), the extreme loads and 1-Hz damage equivalent fatigue loads of fore-aft tower bottom bending moment ($\mathrm{M_{xTB_{max}}}, \mathrm{M_{xTB_{DEL}}}$) and flapwise bending moment at the blade root ($\mathrm{M_{xBC_{min}}}, \mathrm{M_{xBC_{DEL}}}$). Therefore, time-series of 600 s are simulated in the aero-elastic code HAWC2 and load statistics are derived at the location where the strain gauges are installed. A turbulence seed with statistical properties matching those of the measured 10-min conditions is input to the load simulations. The rainflow counting algorithm is used to compute the 1-Hz damage equivalent fatigue loads with Whöler exponent of $m = 12$ for blades and $m = 4$ for the tower. The same approach is used to post-process measured loads. We ~~derive~~ run simulations using wind field characteristics ~~using~~ listed in Table 1, which are derived from both the PL and CW lidars as well as the mast measurements~~for free wind conditions. We refer to the mast-based load predictions in free wind as reference case, also denoted by $\Delta_{R,Ref}$ in the following text.~~. A more detailed analysis is conducted for partial- and full-wake situations~~, where the influence of~~. Here, we investigate how power and load predictions are influenced by filtered and unfiltered turbulence estimates ~~, small~~ derived in Sect. 4.3, characteristic turbulence length scales ~~, and wind characteristics derived from~~ derived in Sect. 4.2 and wind parameters derived from lidar measurements at several ranges~~are evaluated.~~. We provide detailed scatter plots of measured and predicted load sensors used in the analysis in Figs. C1-C5 in the Appendix. The predictions uncertainties for power production and extreme loads are presented in Table 2, and for fatigue loads in Table 3. We define the lidar-based power and load predictions in free wind as the reference case. Thus, we compare the relative error between the uncertainty indicators derived from wake situations with those from the free wind case. Generally, we observe lower prediction accuracy in partial- and full-wake situations compared to the ~~reference~~ free wind scenario, while in some cases similar uncertainty levels are obtained. The following sections describe the results in details.

4.4.1 Power predictions

Power production levels are overestimated in partial-wake, but underestimated in full-wake ~~within $\Delta_R/\Delta_{R,Ref}\sim$~~ by approximately 4% compared to the free wind case. Larger X_R values are found in full-wake compared to the reference case, although R^2 is above 96%, which indicates a good correlation. ~~Although $\Delta_R/\Delta_{R,Ref}$ drops to~~ We do not observe a significant influence of turbulence intensity levels on power predictions, i.e. by comparing the uncertainties in full-wake between simulations performed with filtered and unfiltered turbulence estimates from the CW lidar in Table 2. In a similar way, small turbulence length scales derived in wakes have a negligible effect on power production levels. The power predictions deviations in partial-wake drop to approximately 1%~~in partial-wake using PL lidar~~, when the PL lidar-estimated wind characteristics using measurements up to 1.3 D ~~, induction effects are dominant at these ranges, leading to lower wind speed estimation. In regard to~~ are used in the simulations. This result indicates the sensitivity of the reconstructed wind field characteristics to the upstream ranges in a strongly inhomogeneous wind field as a partial-wake situation.

4.4.2 Extreme load predictions

The extreme loads $(\mathrm{M_{xTB_{max}}}, \mathrm{M_{xBC_{min}}})$ ~~, we obtain $\Delta_R/\Delta_{R,Ref}\sim 2\%$~~ are both affected by the turbulence levels as well as the turbulence length scale. We obtain similar deviations in partial- and full-wake as per the free wind conditions, when using unfiltered turbulence estimates and length scales extracted in ~~free-wind conditions . Simulations~~ free wind conditions (see Table 2). However, simulations based on filtered turbulence consistently overestimate extreme load levels (~~$\Delta_R/\Delta_{R,Ref}\sim$ 3-7%), whereas simulations with low length scales significantly reduce extreme loads up to $\sim$~~ 3–7%). The effect of a low value for the length scale is noticeable in full-wake situations, where L = 7 m leads to biases of the order of -7% compared to the reference case. Overall, higher X_R values are derived in wakes compared to the reference, while R^2 remains above 89% in all analyzed cases. It should also be noticed that the maximum loads do not increase significantly in wake situations, since the wind speed in the wakes is lower than the free wind (Larsen et al., 2013). ~~Fatigue~~

4.4.3 Fatigue load predictions

The biases of fatigue load predictions in partial-wake~~conditions with~~, using unfiltered turbulence statistics and $L = 35$ m~~show $\Delta_R/\Delta_{R,Ref}$ as low as 3% (see Table 3). The~~, are comparable with the deviations observed in free wind conditions, as seen in Table 3. The error increases when filtered turbulence from the PL lidar is used for the simulations, leading to an underestimation of fatigue loads between 2–5%. The most significant deviations are observed for $\mathrm{M_{xTB_{DEL}}}$ and $\mathrm{M_{xBC_{DEL}}}$ in full-wake conditions. The ~~bias of blade-root and tower-bottom predictions, for~~ simulations based on filtered turbulence measures and $L = 35$ m ~~, are approximately~~ lead to an overestimation of blade-root and tower-bottom predictions by 21% ~~higher in full-wake~~ compared to the ~~reference case. Filtered turbulence estimates~~ free wind case. The filtered turbulence statistics are predicted with the use of the spectral velocity tensor model and ~~statistics~~ are found to be approximately ~~9~~11% higher compared to unfiltered turbulence derived from the Doppler radial velocity spectrum (see Fig. 9-middle). ~~Correspondingly, lower~~ The bias of fatigue load predictions ~~are obtained using~~ drop to approximately 11%, when unfiltered turbulence measures ~~, although $\Delta_R/\Delta_{R,Ref} \cong 11\%$ (see Table 3)~~from the CW lidar are simulated. Overall, extreme and fatigue load predictions show low uncertainty when unfiltered turbulence estimates are used as input in simulations. ~~Furthermore, fatigue~~

Fatigue loads are found to correlate significantly better when a synthetic turbulent field characterized by small length scales is used ~~.~~ (i.e. $L = 7$ m). This is demonstrated by ~~lower~~ improved X_R ~~for $\mathrm{M_{xTB_{DEL}}}$ and $\mathrm{M_{xBC_{DEL}}}$ compared to that~~ and R^2 indicators compared to those resulting from simulations with ~~a large length scale. Indeed~~ $L = 35$ m. Besides, reducing L from 35 m (free-wind conditions) to 7 m (fitted in full-wake conditions) reduces ~~extreme tower-bottom loads by 7% and~~ fatigue blade-root ~~loads~~ load levels by 15%. ~~These results show the~~ The simulations with low length scales and unfiltered turbulence measures provide the lowest deviations in full-wake compared to the reference case, as the error drops to -4% for $\mathrm{M_{xBC_{DEL}}}$~~,~~, indicating underprediction (see Table 3). These results demonstrate the improved accuracy of load predictions when unfiltered turbulence measures are simulated, and validate the importance of characterizing turbulence spectral parameters for load analysis~~,~~; as previously demonstrated in Thomsen and Sørensen (1998), Sathe et al. (2012), and Dimitrov et al. (2017). ~~A decrease in the turbulence length scale leads to a shift of the Mann spectrum towards higher wavenumbers, whereas the opposite is seen for increase length scale (Dimitrov et al., 2017). The shift of the spectrum determine the turbulence energy content corresponding to the range of frequencies of the rotor harmonics, which affects the magnitude of the loading conditions. The simulations with low length scales and unfiltered turbulence measures show improved accuracy, as $\Delta_R/\Delta_{R,Ref} < 4\%$ for $\mathrm{M_{xTB_{DEL}}}$ and $\mathrm{M_{xBC_{DEL}}}$ in full-wake conditions. The inter-comparison of uncertainties of the analyzed load sensors obtained with PL and CW lidars' reconstructed parameters, based on same flow modelling assumptions, reveal deviations of X_R, R^2 and Δ_R within 3%.~~

4.5 Sensitivity ~~analysis~~of inflow parameters on load predictions

We use a first order polynomial response surface for evaluating the sensitivity of the predictions with respect to input wind variables. We consider ~~$\bar{u}, \sigma_U/U, \alpha, \Delta\varphi, \bar{\varphi}, L$~~ $\bar{u}, \sigma_u/u, \alpha, \Delta\varphi, \bar{\varphi}, L$ in the analysis. The first-order polynomials are separately fitted for free-, partial- and full-wake conditions based on the PL lidar-measured wind field parameters. We ensure close to 850 10-min samples for each case. Besides, L is assumed to randomly vary between 7 and 30 m in full-wake and between 15

Table 2. List of accuracy and uncertainty values for power and extreme load validation procedures. The marker ** indicates unfiltered turbulence obtained from the ensemble-average Doppler spectrum of the radial velocity at 1.3 D.

Case	Sensor / ranges	Mann's length scale L [m]	$\mathrm{Power_{mean}}$			$\mathrm{MxTB_{max}}$			$\mathrm{MxBC_{min}}$		
			R^2	X_R	Δ_R	R^2	X_R	Δ_R	R^2	X_R	Δ_R
Wake-free	Mast ~~(reference)~~	35	0.99	0.09	1.01	0.97	0.09	0.97	0.96	0.09	0.99
	PL (0.7 D - 2.5 D)		0.99	0.09	1.01	0.97	0.09	0.98	0.96	0.09	1.01
	CW (1.0 D - 2.5 D)		0.99	0.09	0.98	0.97	0.09	0.95	0.97	0.08	1.01
Partial-Wake	PL (0.7 D - 2.5 D)	35	0.99	0.10	1.05	0.91	0.12	1.00	0.91	0.12	1.05
	PL (0.7 D - 1.3 D)		0.99	0.09	1.02	0.92	0.11	0.98	0.92	0.11	1.02
	CW (1.0 D - 2.5 D)**		0.99	0.10	1.03	0.92	0.11	0.97	0.92	0.10	1.01
	PL (0.7 D - 2.5 D)	15	0.99	0.09	1.06	0.91	0.11	0.97	0.91	0.11	1.02
	CW (1.0 D - 2.5 D)**		0.99	0.10	1.04	0.92	0.11	0.96	0.93	0.10	0.99
Full-Wake	PL (0.7 D - 2.5 D)	35	0.97	0.19	0.95	0.92	0.14	0.99	0.91	0.12	1.06
	CW (1.0 D - 2.5 D)		0.96	0.17	0.96	0.89	0.14	0.98	0.89	0.12	1.05
	CW (1.0 D - 2.5 D)**		0.96	0.18	0.95	0.90	0.14	0.95	0.89	0.12	1.01
	PL (0.7 D - 2.5 D)	7	0.97	0.18	0.95	0.90	0.14	0.92	0.91	0.12	0.98
	CW (1.0 D - 2.5 D)		0.97	0.15	0.96	0.92	0.13	0.91	0.91	0.10	0.97
	CW (1.0 D - 2.5 D)**		0.97	0.16	0.95	0.91	0.14	0.89	0.91	0.11	0.94

and 35 m in partial-wake and free-wake situations. We normalize the input variables such that their values are scaled between zero and one to allow the sensitivity study. The obtained linear regression coefficients for $\mathrm{Power_{mean}}$, $\mathrm{M_{xBC_{DEL}}}$ and $\mathrm{M_{xTB_{max}}}$ responses are presented in Fig. 10. The power predictions are strongly driven by the reconstructed mean wind speed at hub height as shown in Fig. 10 (left). This indicates that the observed Δ_R values in Table 2 are mostly explained by the uncertainty in the wind speed reconstruction. The mean wind speed and turbulence intensity have the largest influence on the fatigue load predictions (see Fig.10-middle). In comparison to the wake-free scenario, we observe the ~~increase~~ increased effect of turbulence intensity and reduced influence of shear exponents in wake situations. This is due to the significantly high turbulence levels measured inside the wakes (up to 1.8 times higher than under free-wind conditions) and relatively low shear exponent values (see Fig. 6). The former is a well-known fatigue load driver. The latter implies small velocity gradients within the rotor area, which lead to lower blade-root fatigue loads (Sathe et al., 2012; Dimitrov et al., 2015). The effects of α, $\Delta\varphi$, $\bar{\varphi}$, and L are secondary compared to $\bar{u}$ and $\cancel{\sigma_U/U}$ σ_u/u. We observe slightly higher sensitivity of L in full-wake compared to partial-wake and free-wind conditions. However, according to the results in Table 3, the length scale parameter has a significant impact on loads when assessed independently. Finally, $\bar{u}$ and $\cancel{\sigma_U/U}$ σ_u/u have the largest influence on the extreme tower bottom loads in Fig. 10 (right). Overall, the order of importance of the analyzed inflow parameters are comparable with the more detailed sensitivity studies provided in Dimitrov et al. (2018).

Table 3. ~~Similar to Table 2 but~~ List of accuracy and uncertainty values for fatigue load validation procedures. The marker ** indicates unfiltered turbulence obtained from the ensemble-average Doppler spectrum of the radial velocity at 1.3 D.

Case	Sensor / ranges	Mann's length scale L [m]	MxTB$_{\mathrm{DEL}}$			MxBC$_{\mathrm{DEL}}$		
			R^2	X_R	Δ_R	R^2	X_R	Δ_R
Wake-free	Mast ~~(reference)~~	35	0.86	0.19	0.93	0.84	0.22	1.01
	PL (0.7 D - 2.5 D)		0.85	0.20	0.97	0.83	0.23	1.09
	CW (1.0 D - 2.5 D)		0.86	0.18	0.91	0.84	0.21	1.01
Partial Wake	PL (0.7 D - 2.5 D)	35	0.81	0.18	0.95	0.83	0.23	1.04
	PL (0.7 D - 1.3 D)		0.82	0.18	0.93	0.83	0.22	1.02
	CW (1.0 D - 2.5 D)**		0.80	0.17	0.92	0.85	0.19	1.00
	PL (0.7 D - 2.5 D)	15	0.83	0.17	0.94	0.83	0.21	0.98
	CW (1.0 D - 2.5 D)**		0.83	0.16	0.90	0.86	0.17	0.94
Full Wake	PL (0.7 D - 2.5 D)	35	0.78	0.19	1.11	0.84	0.24	1.22
	CW (1.0 D - 2.5 D)		0.74	0.18	1.08	0.81	0.20	1.19
	CW (1.0 D - 2.5 D)**		0.73	0.17	1.01	0.80	0.19	1.12
	PL (0.7 D - 2.5 D)	7	0.82	0.15	1.09	0.85	0.18	1.07
	CW (1.0 D - 2.5 D)		0.79	0.16	1.05	0.84	0.16	1.02
	CW (1.0 D - 2.5 D)**		0.79	0.16	0.97	0.84	0.15	0.97

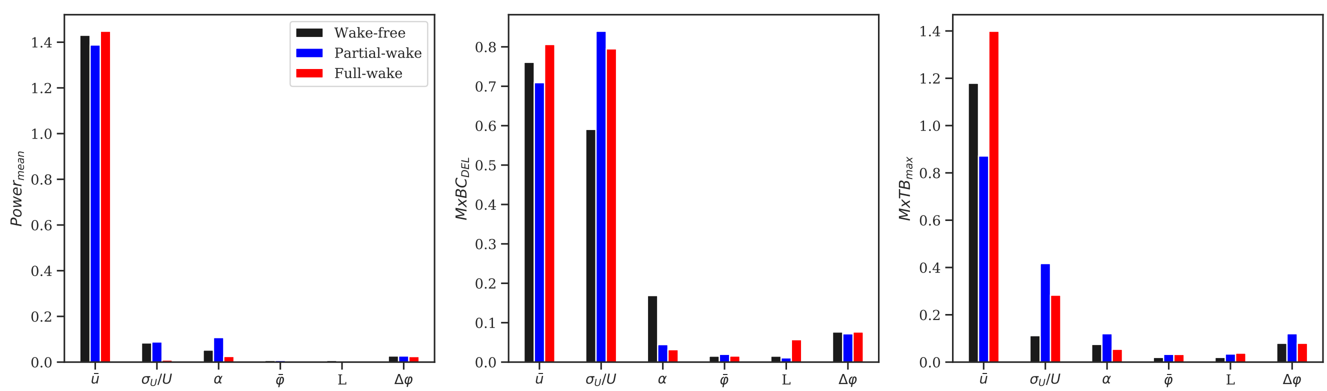

Figure 10. Regression coefficients of a linear response surface model identifying the sensitivity of wind field parameters on selected load sensors.

~~We provide detailed scatter plots of measured and predicted load sensors used in the analysis in Figs. C1-C5 in the Appendix. We~~

4.5.1 Uncertainty distribution as function of wind speed

We analyze the bias and uncertainty of $\mathrm{Power_{mean}}, \mathrm{M_{xBC_{DEL}}}, \mathrm{M_{xTB_{max}}}$ predictions with respect to the inflow wind speed in Fig. 11. We observe larger deviations of the selected sensors at low wind speeds, which gradually decrease for higher winds. The deviations in the reference case (black line) and wake situations are a combination of uncertainty in the reconstructed wind profiles, aero-elastic model uncertainty, load measurement uncertainty as well as statistical uncertainty (Dimitrov et al., 2019). Although there is not sufficient information to distinguish among the various uncertainty sources, we assume that the deviations are due to the error in the wind field representation only. The power predictions uncertainties with respect to mean wind speed in free-, partial- and full-wake situations are plotted in Fig. 11 (left). We observe a consistent overprediction of power levels in partial-wake conditions (blue line) and underprediction in full-wake conditions (red line) for the full range of wind speeds. The predictions of $\mathrm{M_{xBC_{DEL}}}$ with respect to the mean wind speeds in free- and full-wake conditions are plotted in Fig.11 (middle). The predictions based on the unfiltered turbulence (green line) show better agreement to the reference compared to results based on filtered turbulence (red line). It is also found that largest deviations occur at low wind speeds ($\bar{u} < 8$ m/s). Finally, we show the results using unfiltered turbulence and low length scale (purple line), which provide the lowest error. The residual deviations can be partly explained by the uncertainty in turbulence statistics and spectral properties representation. Figure 11 (right) shows that comparable deviations are obtained for tower extreme loads in partial- and full-wake situations as for the reference case.

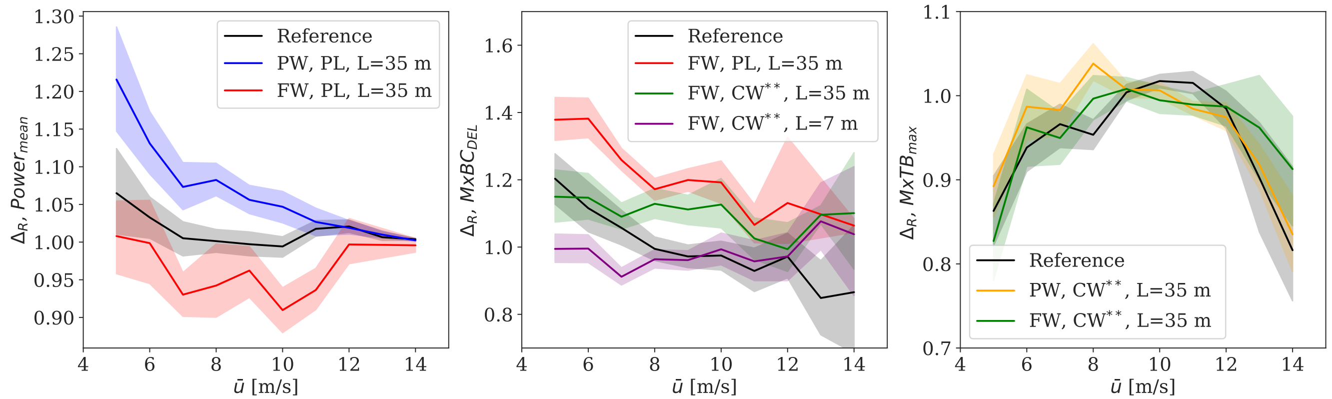

Figure 11. Comparison of bias (solid line) and uncertainty (error band) of selected load sensors with respect to inflow mean wind speed. The analyzed cases are shown with coloured lines in each sub-plot. The reference case denotes the mast-based free wind scenario; PW refers to partial-wake and FW refers to full-wake conditions. We show results from both PL and CW lidars and different turbulence length scales L. The marker ** indicates unfiltered turbulence obtained from the ensemble-average Doppler spectrum of the radial velocity at 1.3 D.

5 Discussion

Wind field parameters used as inputs for aero-elastic simulations are derived from PL and CW lidar measurements of the wake field behind an operating wind turbine. Although the two lidars follow different scanning patterns and the wake flow field is strongly inhomogeneous, we find a very good agreement between the PL and CW lidar-estimated horizontal wind speed and filtered turbulence in partial- and full-wake situations. The estimation of the wind veer, yaw error and shear exponent using nacelle-mounted lidars is prone to high level of uncertainty and is affected by the scanning patterns. This is demonstrated by the larger scatter between the estimated parameters by the PL and CW lidars in wake compared to free-wind conditions (not shown). However, we demonstrate that the influence of these parameters on the loads and power predictions is minor compared to mean wind speed, turbulence intensity and length scale. Although the present work does not focus in details on the performance of the two lidar systems, the findings indicate that the main sources of uncertainty in load predictions are related to flow modelling assumptions. ~~Power production levels are highly dependent on the estimated mean wind speed at hub height. The observed power prediction's deviations~~ The wind velocity gradient in the wake is characterized by the combined effect of the atmospheric shear and the wake deficit. The former can be explained by a power law profile, while the latter is often approximated in the far wake by a Gaussian function, whose depth and width depend on ambient conditions and turbine operation regimes (Aitken et al., 2014). Further, the 10-min average wind velocity gradient, observed from a fixed point, will be largely influenced by wake meandering in the lateral and vertical directions increasing the complexity of the velocity field in the wake region. The results of the power prediction's deviations in Table 1, in both partial- and full-wake situations, indicate ~~an inaccurate~~ a less accurate reconstruction of the ~~mean wind speed. More precisely, the flow modelling assumptions, including horizontal homogeneous wind flow, power law vertical wind profile and linear veer within the scanned areas, introduce larger errors in wake than~~ wind field when compared to wake-free conditions. ~~Furthermore, we do not distinguish situations where the lidar beams are partly measuring inside the wake and partially outside to reconstruct the inflow wind field. This could be resolved if wake characteristics as shape, depth and center position are integrated in the WFR techniques (Trujillo et al., 2011). Deriving a rotor equivalent wind speed model, which accounts for velocity gradients as well as wake characteristics is necessary to~~ Although we demonstrate a low sensitivity of the loads to the shear exponent for all the analysed sensors (see Fig. 10), it is envisioned to more appropriately account for wake-affected velocity gradient profiles and determine whether or not this will significantly improve the accuracy of power and load predictions. It is ~~also important to point out that, in the region of high velocity gradients as wake edges, the probe volume averaging effects can lead to significant errors in the estimation of the mean wind speed (Lundquist et al., 2015; Meyer Forsting et al., 2017).~~

~~It is~~ well-established that fatigue loads are dominated by turbulence levels. However, to extract turbulence parameters by combining a turbulence model with a model of the spatial radial velocity averaging of the lidars introduces significant uncertainty under wake conditions. Indeed, filtered turbulence estimates in wakes are 6–10% higher than unfiltered turbulence measures, derived from the Doppler radial velocity spectrum, as shown in Figs. 8 and 9. We describe the wake flow as a homogeneous field by using the Mann spectral tensor model fitted using PL lidar measurements at hub height. Nonetheless, wake fields are highly inhomogeneous and spectral properties vary significantly within the rotor region (Kumer et al., 2017).

We derive turbulence length scales in wakes and demonstrate the importance of characterizing turbulence spectra for the load analysis. The observed magnitude of decrease in longitudinal turbulence length scale is consistent with results reported in Thomsen and Sørensen (1998) and Madsen et al. (2010), where wake-added turbulence is characterized by length scales within the range 10–25% of the free wind length scale. However, a detailed analysis including atmospheric stability effects on both turbulence spectra and wake characteristics can potentially reduce the uncertainty of load predictions (Sathe et al., 2012; Dimitrov et al., 2017). Furthermore, cross-contamination effects and probe volume averaging effects become larger in wakes, as the size of turbulence eddies decrease to length scales comparable or lower than the lidar probe volume. These effects increase the uncertainty of extracted turbulence length scales from lidar measurements. Despite this, fatigue load predictions show significant improvement by using low turbulent length scales; spectral analysis of measured and predicted loads is required for a better understanding of the accuracy of the lidar-fitted synthetic turbulence field in wakes.

We demonstrate that improved fatigue load predictions are obtained using unfiltered turbulence measures from the Doppler radial velocity spectrum. However, the estimation of σ_U^2 from the σ_{LOS}^2 relies on flow homogeneity and Taylor's frozen turbulence hypothesis (Taylor, 1938). These assumptions are sound for large-scale wind fluctuations and free flow over flat and homogeneous terrain, but not valid in wakes (Schlipf et al., 2010). The current wind field modelling approach omits the large-scale meandering of wakes, which has strong impact on power and load predictions (Larsen et al., 2013). These uncertainty sources, among others, can partially explain the observed deviations.

The influence of wake effects on power and load levels depend on the wind farm layout, ambient wind speed and turbulence, and atmospheric stratification, among others. The current state-of-the-art approach to predict wake flows and their influence on wind turbine operations relies on engineering-like wake models (Frandsen, 2007; Madsen et al., 2010). These models ensure an acceptable level of accuracy, robustness and computational cost. Previous studies carried out load validation using the effective turbulence model and the DWM model, which are recommended in the IEC 61400-1. The inter-comparison of the two models showed fatigue load prediction deviations of 20% (Thomsen et al., 2007). ~~The effective turbulence approach under predicted fatigue load levels at spacings larger than 5 D (Schmidt et al., 2011). Although the DWM model~~ Although DWM-based power and load predictions showed a very fine agreement ~~between power and load predictions in wake conditions (Larsen et al., 2013), these studies did not quantify uncertainty~~ with measurements collected in a wind farm (Larsen et al., 2013), the uncertainty of the predictions was not quantified in a systematic approach. Recently, ~~Reinwardt et al. (2018) estimated fatigue load biases~~ the work of Reinwardt et al. (2018) quantified deviations between DWM-based and measured fatigue loads in the range of 11–15% for the tower bottom and 8–21% for the ~~flapwise bending blade using the DWM~~blade-root flapwise bending moment. Results from earlier studies show deviations of the same or even larger order of magnitude compared to the results from our load validation approach. Despite of the discussed shortcomings, load validation under wake conditions based on lidar measurements may be already a viable alternative to the engineering wake models. We will soon evaluate whether the differences in the calculated loads using lidar-estimated wind characteristics in wakes are larger compared to the uncertainties in the load calculations with state-of-the-art wake models such as DWM.

6 Conclusions

We demonstrated a procedure for carrying out load validation in partial- and full-wake conditions using measurements from two types of forward-looking nacelle lidars: a pulsed and continuous wave system. The suggested procedure characterized wake-induced effects by means of lidar-reconstructed wind field parameters commonly used as input for load simulations~~. These parameters were reconstructed using lidar measurements of the wake flow field~~, without applying wake deficit models. We considered the uncertainty of ~~load predictions in wake-free sectors using mast-measured~~ lidar-based load predictions against wind turbine on-board sensors in free wind conditions as ~~the~~ reference case. ~~We~~ Hence, we quantified the uncertainty ~~and bias of power and load predictions in partial- and full-wake conditionsusing lidar-estimated wind field characteristics~~of lidar-based load predictions against sensors data in wake conditions, and compared it to uncertainty of the free wind case. The reconstructed mean wind speed, turbulence intensity as well as the turbulence length scale in wake conditions were found to be the most influential parameters on the predictions.

Power production levels under wake conditions were strongly ~~related to the mean~~ driven by the reconstructed wind speed at hub height, whereas ~~the vertical and horizontal wind profiles~~ turbulence intensity as well as turbulence length scales had negligible effects on those levels. Power predictions ~~in partial- and~~ were overestimated in partial-wake, but underestimated in full-wake ~~conditions deviated up to~~ by approximately 4% compared to the ~~reference case~~free wind conditions. Fatigue loads were affected by turbulence characteristics inside the wake. The use of a spectral velocity tensor model to derive turbulence parameters introduced significant uncertainty under wake conditions. The tower-bottom and blade-root bending moments predictions ~~deviated by 3% in partial-wake conditions, and~~ were overestimated by 21% in full-wake conditions using filtered turbulence measures and turbulence length scales typical of free-wind conditions. The ~~simulation bias in full-wake conditions~~ bias was reduced to 11% using unfiltered turbulence measures derived from the ensemble-average Doppler radial velocity spectrum. ~~The~~ Overall, the measured and predicted fatigue and extreme loads were found to correlate significantly better when a synthetic turbulent field characterized by a low turbulence length scale was used. Furthermore, simulations with low turbulence length scales led to ~~a strong reduction of load levels, reducing the bias of fatigue loads to~~ uncertainty levels of blade-root fatigue load predictions of the order of 4% ~~under wake conditions~~compared to the free-wind case. However, estimating turbulence characteristics under wake conditions using measurements from nacelle-mounted lidars was prone to high level of uncertainty due to probe volume effects and flow modelling assumptions. ~~We~~ The present work demonstrated the applicability of nacelle-mounted lidar measurements to extend load and power validations under wake conditions and highlighted the main challenges. Further investigation is necessary to verify that the observed uncertainty of predictions are comparable with results using state-of-the-art wake models recommended by the IEC standard. Future research should apply a wind deficit model that accounts for the combined effect of atmospheric shear and wake deficit, and quantify the uncertainty of resulting power and load predictions.

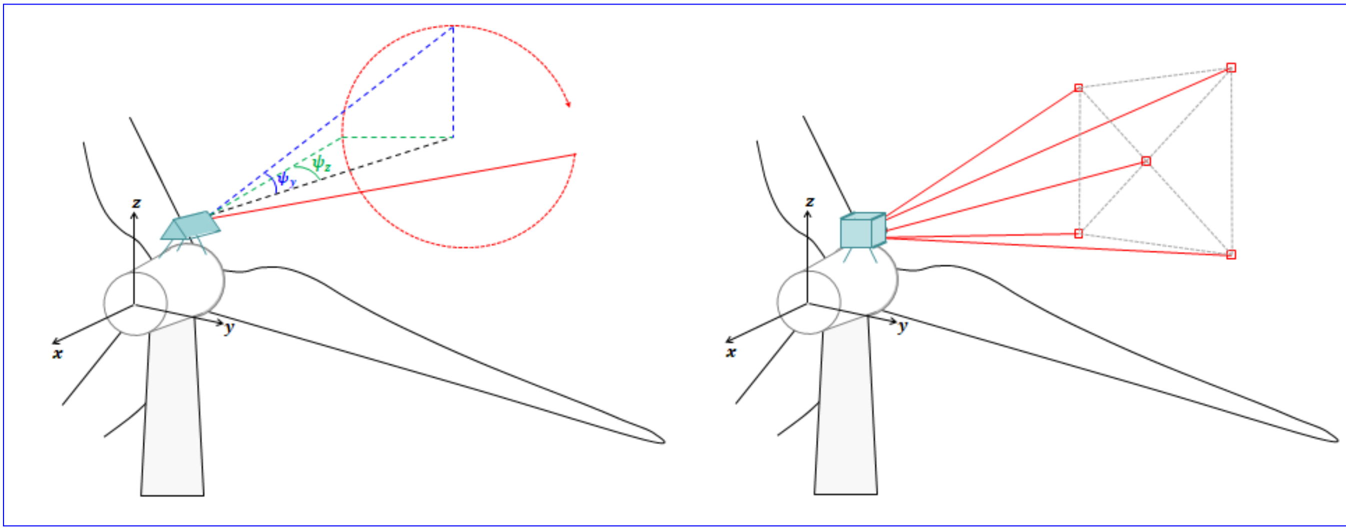

Figure A1. Schematic view of the measurement patterns of nacelle-mounted lidars: CW lidar (left) and PL lidar (right).

Appendix A: Schematic view of the nacelle-mounted lidars measurement patterns

Appendix B: Wake detection from mast measurements

The wake detection algorithm (see Sect. 3.4) is extended to the mast measurements to classify 10-min periods where the mast is in free or wake situations. For this purpose, turbulence observations from the cup anemometer at 80 m and vertical wind shear computed using the measurements from the cup anemometers at 57.5 and 80 m are used as wake detection parameters. Their $99th$ percentiles are used as conservative thresholds to characterize the limits of the normal range of the site-specific free wind conditions. The resulting thresholds are $TI_{mast,99} = 0.20$ and $\alpha_{mast,99} = -0.02$. If one of the two limits is exceeded within a 10-min period, the mast is considered in wake conditions and shown with green markers in Fig. B1.

Appendix C: Figures with load statistics comparisons

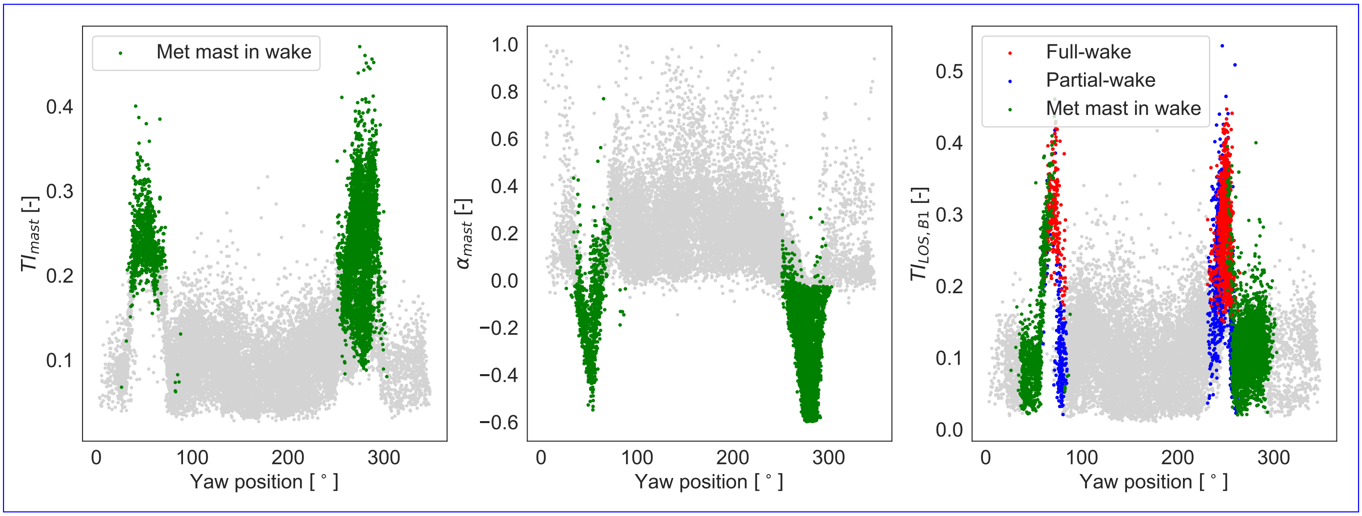

Figure B1. Left and middle: 10-min observations of the turbulence intensity and vertical wind shear at the mast as function of turbine yaw position. Free wind conditions relative to the mast are identified with grey markers, and waked situations with green markers. Right: PL-estimated 10-min wake detection parameter $TI_{LOS,B1}$. Detected wake situations of turbine T04 are shown with coloured markers: wake-free (grey), partial-wake (blue) and full-wake (red). The 10-min periods, where the mast is affected by wakes are shown in green markers.

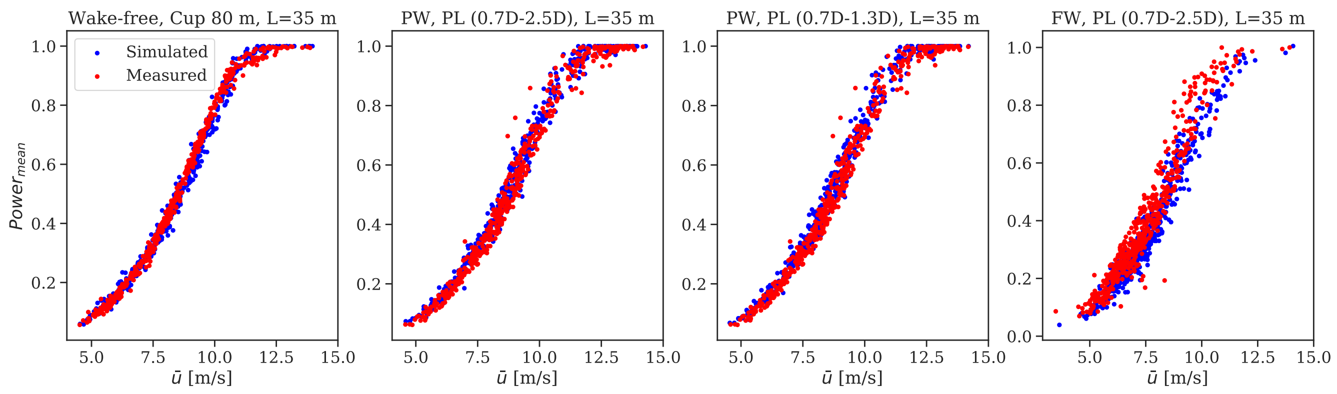

Figure C1. Scatter plots of the normalized measured and predicted power mean realizations used in the analysis.

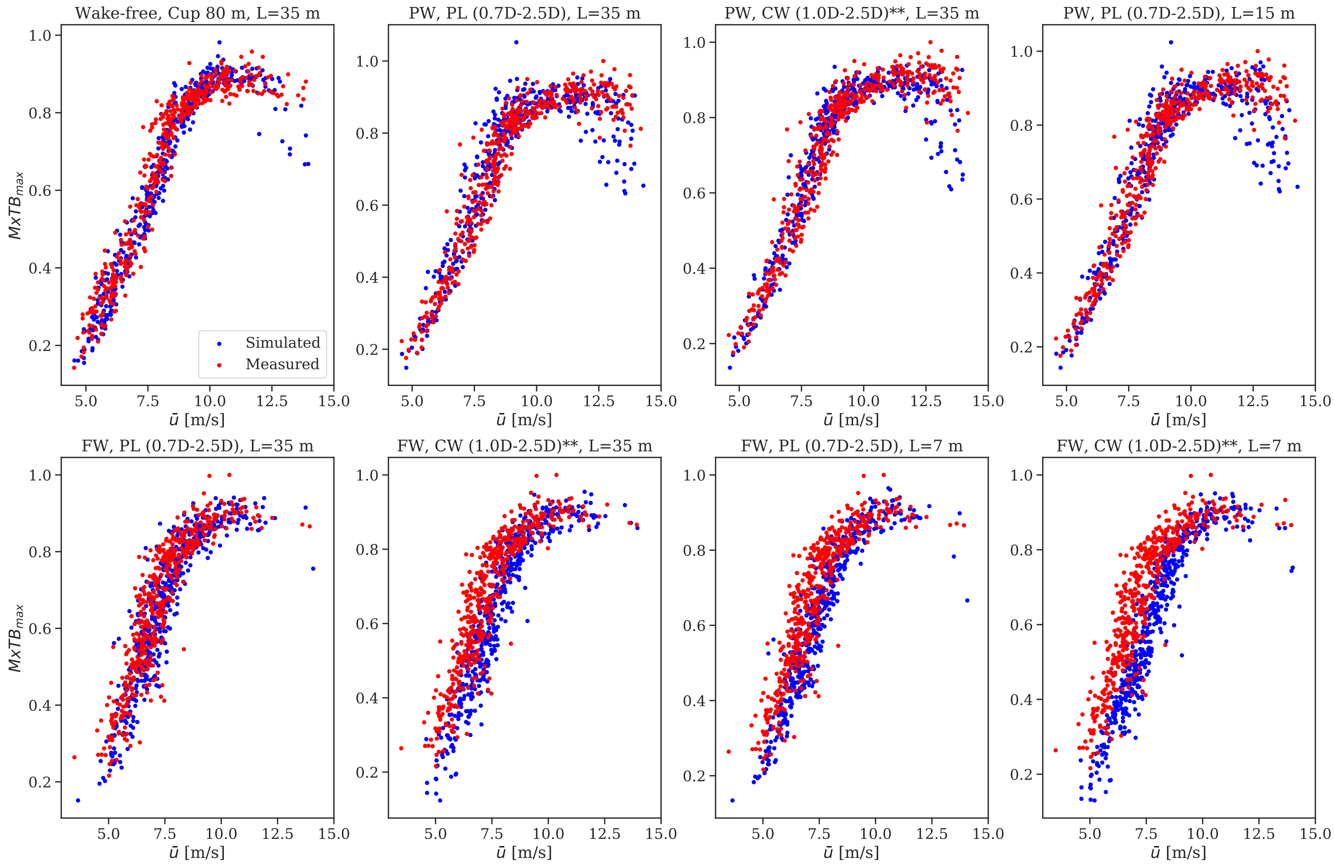

Figure C2. Scatter plots of the normalized measured and predicted extreme fore-aft tower bottom bending moment realizations used in the analysis.

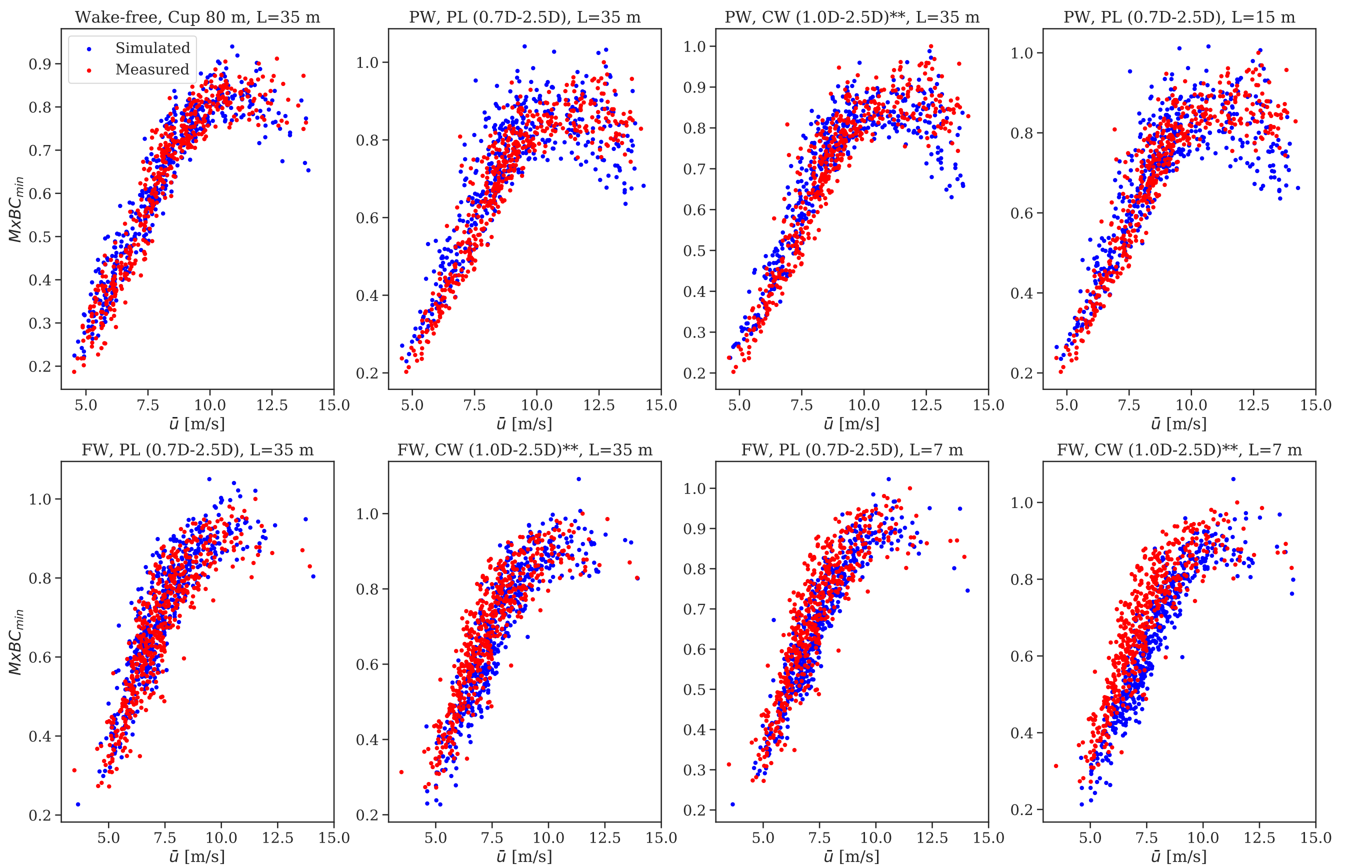

Figure C3. Scatter plots of the normalized measured and predicted extreme flapwise bending moment at the blade root realizations used in the analysis.

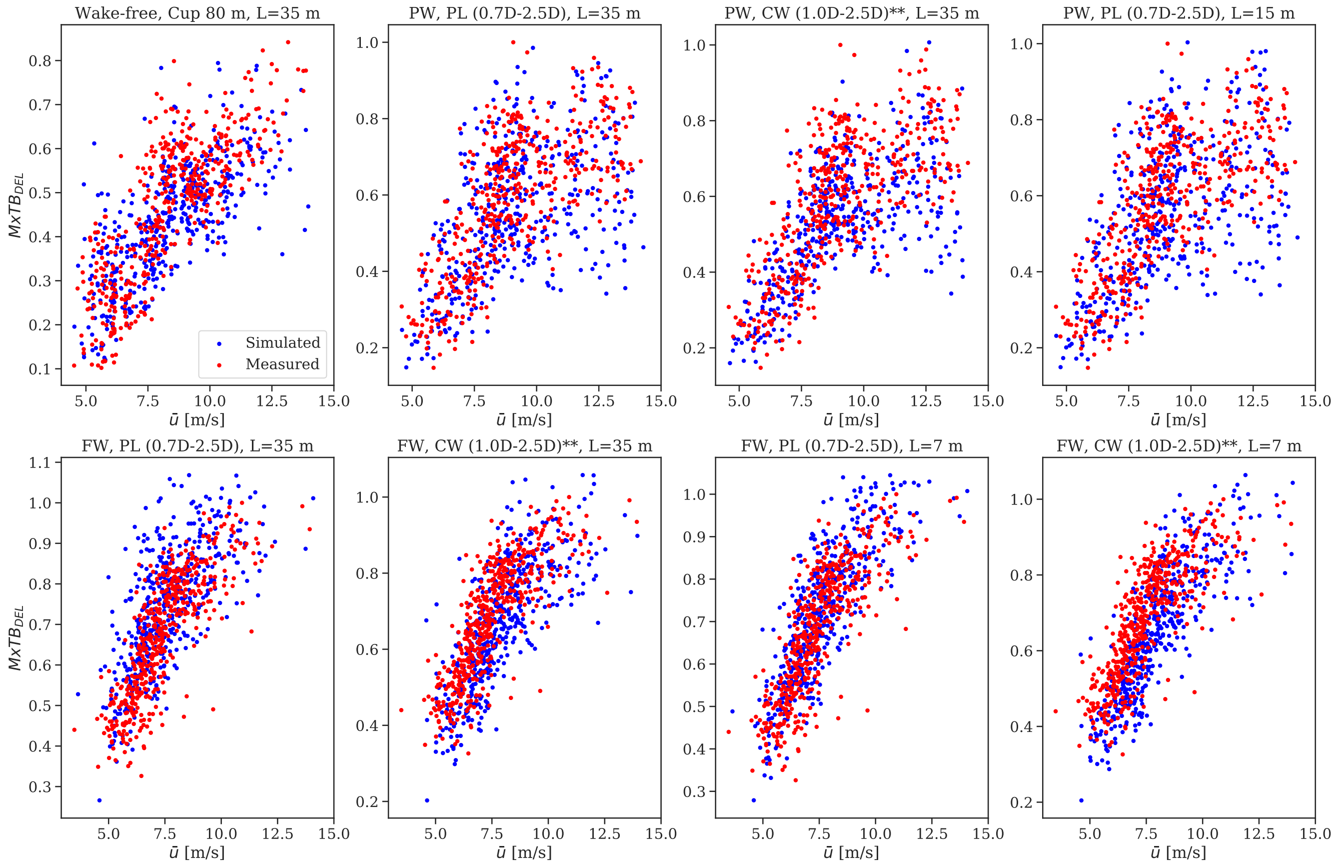

Figure C4. Scatter plots of the normalized measured and predicted fatigue fore-aft tower bottom bending moment realizations used in the analysis.

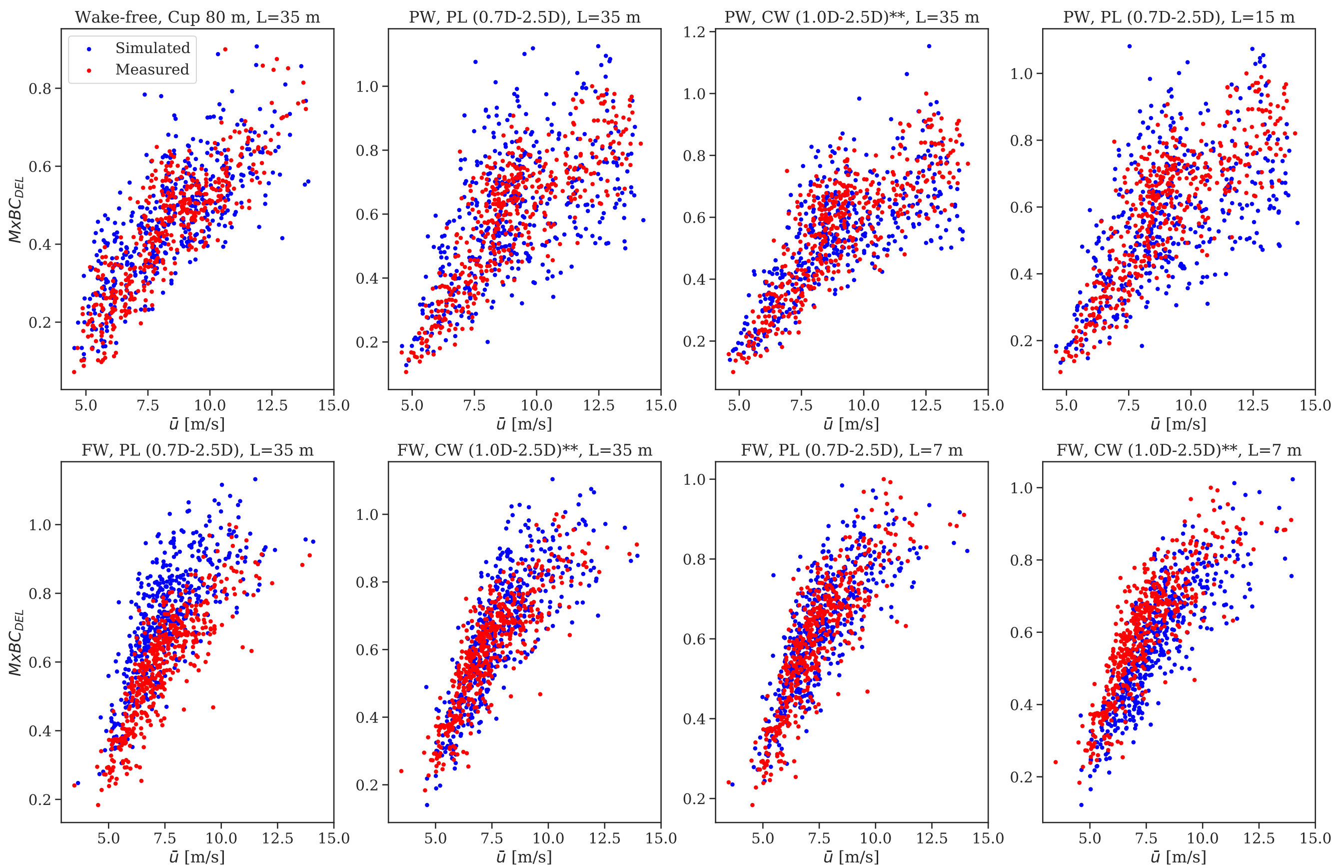

Figure C5. Scatter plots of the normalized measured and predicted fatigue flapwise bending moment at the blade root realizations used in the analysis.

Data availability. Turbine data are not publicly available because there is a non-disclosure agreement between the partners in the UniTTe project. Lidar and mast data can be requested from Rozenn Wagner at DTU Wind Energy (rozn@dtu.dk).

Competing interests. The authors declare that they have no conflict of interest.

Acknowledgements. Special thanks to Rozenn Wagner for making the NKE dataset available for our study. Thanks to the lidar manufacturers from Avent and ZephIR for providing their systems. Thanks to Vattenfall and Siemens Gamesa Renewable Energy for providing the site and turbine to conduct the measurement campaign

References

International Standard IEC61400-13: Wind turbines - Part 13: Measurement of mechanical loads, Standard, IEC, 2015.

International Standard IEC61400-12-1: Wind energy generation systems - Part 12-1: Power performance measurements of electricity producing wind turbines, Standard, IEC, 2017.

International Standard IEC61400-1: wind turbines—part 1: design guidelines, Fourth; 2019, Standard, IEC, 2019.

Aitken, M. L. and Lundquist, J. K.: Utility-scale wind turbine wake characterization using nacelle-based long-range scanning lidar, Journal of Atmospheric and Oceanic Technology, 31, 1529–1539, https://doi.org/10.1175/JTECH-D-13-00218.1, 2014.

Aitken, M. L., Banta, R. M., Pichugina, Y. L., and Lundquist, J. K.: Quantifying wind turbine wake characteristics from scanning remote sensor data, Journal of Atmospheric and Oceanic Technology, 31, 765–787, https://doi.org/10.1175/jtech-d-13-00104.1, 2014.

Bingöl, F., Mann, J., and Larsen, G. C.: Light detection and ranging measurements of wake dynamics Part I: One-dimensional Scanning, Wind Energy, 13, 51–61, https://doi.org/10.1002/we.352, 2010.

Borraccino, A. and Courtney, M.: Calibration report for ZephIR Dual Mode lidar (unit 351), 2016a.

Borraccino, A. and Courtney, M.: Calibration report for Avent 5-beam Demonstrator lidar, 2016b.

Borraccino, A., Schlipf, D., Haizmann, F., and Wagner, R.: Wind Field Reconstruction from Nacelle-Mounted Lidars Short Range Measurements, Wind Energy Science, 2, 269–283, https://doi.org/10.5194/wes-2017-10, 2017.

Branlard, E., Pedersen, A. T., Mann, J., Angelou, N., Fischer, A., Mikkelsen, T., Harris, M., Slinger, C., and Montes, B. F.: Retrieving wind statistics from average spectrum of continuous-wave lidar, Atmospheric Measurement Techniques, 6, 1673–1683, https://doi.org/10.5194/amt-6-1673-2013, 2013.

Chamorro, L. P., Guala, M., Arndt, R. E., and Sotiropoulos, F.: On the evolution of turbulent scales in the wake of a wind turbine model, Journal of Turbulence, 13, 1–13, https://doi.org/10.1080/14685248.2012.697169, 2012.

Dimitrov, N., Natarajan, A., and Kelly, M.: Model of wind shear conditional on turbulence and its impact on wind turbine loads, Wind Energy, 18, 1917–1931, https://doi.org/10.1002/we.1797, https://onlinelibrary.wiley.com/doi/abs/10.1002/we.1797, 2015.

Dimitrov, N., Borraccino, A., Peña, A., Natarajan, A., and Mann, J.: Wind turbine load validation using lidar-based wind retrievals, Wind Energy, 22, 1512–1533, https://doi.org/10.1002/we.2385, 2019.

Dimitrov, N. K., Natarajan, A., and Mann, J.: Effects of normal and extreme turbulence spectral parameters on wind turbine loads, Renewable Energy, 101, 1180–1193, https://doi.org/10.1016/j.renene.2016.10.001, 2017.

Dimitrov, N. K., Kelly, M. C., Vignaroli, A., and Berg, J.: From wind to loads: wind turbine site-specific load estimation with surrogate models trained on high-fidelity load databases, Wind Energy Science, 3, 767–790, https://doi.org/10.5194/wes-3-767-2018, 2018.

Frandsen, S. T.: Final report on measurements on and modelling of offshore wind farms, Risø National Laboratory, 1996.

Frandsen, S. T.: Turbulence and turbulence-generated structural loading in wind turbine clusters, Risø National Laboratory, 2007.

Frehlich, R.: Scanning doppler lidar for input into short-term wind power forecasts, Journal of Atmospheric and Oceanic Technology, 30, 230–244, https://doi.org/10.1175/jtech-d-11-00117.1, 2013.

Hansen, M., Gaunaa, M., and Aagaard Madsen, H.: A Beddoes-Leishman type dynamic stall model in state-space and indicial formulations, 2004.

Held, D. P. and Mann, J.: Detection of wakes in the inflow of turbines using nacelle lidars, Wind Energy Science, 4, 407–420, https://doi.org/10.5194/wes-4-407-2019, 2019.

Iungo, G. V. and Porté-Agel, F.: Volumetric lidar scanning of wind turbine wakes under convective and neutral atmospheric stability regimes, Journal of Atmospheric and Oceanic Technology, 31, 2035–2048, https://doi.org/10.1175/jtech-d-13-00252.1, 2014.

Kim, T., Hansen, A. M., and Branner, K.: Development of an anisotropic beam finite element for composite wind turbine blades in multibody system, Renewable Energy, 59, 172–183, https://doi.org/10.1016/j.renene.2013.03.033, 2013.

Kumer, V.-M., Reuder, J., and Oftedal Eikill, R.: Characterization of Turbulence in Wind Turbine Wakes under Different Stability Conditions from Static Doppler LiDAR Measurements, Remote Sensing, 9, 242 (20 pp.), 242 (20 pp.), https://doi.org/10.3390/rs9030242, 2017.

Larsen, G. C., Madsen, H. A., Thomsen, K., and Larsen, T. J.: Wake meandering - a pragmatic approach, 2006.

Larsen, G. C., Madsen, H. A., Bingöl, F., Mann, J., Ott, S., Sørensen, J., Okulov, V., Troldborg, N., Nielsen, N. M., Thomsen, K., Larsen, T. J., and Mikkelsen, R.: Dynamic wake meandering modeling, 2007.

Larsen, G. C., Madsen, H. A., Larsen, T. J., and Troldborg, N.: Wake modeling and simulation, 2008.

Larsen, T. J. and Hansen, A. M.: How 2 HAWC2, the user's manual, Risø National Laboratory, 2007.

Larsen, T. J., Madsen, H. A., Larsen, G. C., and Hansen, K. S.: Validation of the dynamic wake meander model for loads and power production in the Egmond aan Zee wind farm, Wind Energy, 16, 605–624, https://doi.org/10.1002/we.1563, 2013.

Lundquist, J. K., Churchfield, M. J., Lee, S., and Clifton, A.: Quantifying error of lidar and sodar doppler beam swinging measurements of wind turbine wakes using computational fluid dynamics, Atmospheric Measurement Techniques, 8, 907–920, https://doi.org/10.5194/amt-8-907-2015, 2015.

Machefaux, E., Larsen, G. C., Troldborg, N., Hansen, K. S., Angelou, N., Mikkelsen, T., and Mann, J.: Investigation of wake interaction using full-scale lidar measurements and large eddy simulation, Wind Energy, 19, 1535–1551, https://doi.org/10.1002/we.1936, 2016.

Madsen, H. A., Larsen, G. C., Larsen, T. J., Troldborg, N., and Mikkelsen, R. F.: Calibration and Validation of the Dynamic Wake Meandering Model for Implementation in an Aeroelastic Code, Journal of Solar Energy Engineering, 132, 041 014, https://doi.org/10.1115/1.4002555, 2010.

Mann, J.: The spatial structure of neutral atmospheric surface-layer turbulence, Journal of Fluid Mechanics, 273, 141–168, 1994.

Mann, J.: Wind field simulation, Probabilistic Engineering Mechanics, 13, 269–282, https://doi.org/10.1016/S0266-8920(97)00036-2, 1998.

Mann, J., Cariou, J.-P., Courtney, M., Parmentier, R., Mikkelsen, T., Wagner, R., Lindelöw, P. J. P., Sjöholm, M., and Enevoldsen, K.: Comparison of 3D turbulence measurements using three staring wind lidars and a sonic anemometer, Meteorologische Zeitschrift, 18, 135–140, https://doi.org/10.1127/0941-2948/2009/0370, 2009.

Mann, J., Peña, A., Bingöl, F., Wagner, R., and Courtney, M.: Lidar Scanning of Momentum Flux in and above the Atmospheric Surface Layer, Journal of Atmospheric and Oceanic Technology, 27, 959–976, https://doi.org/10.1175/2010jtecha1389.1, 2010.

Mann, J., Peña, A., Troldborg, N., and Andersen, S. J.: How does turbulence change approaching a rotor?, Wind Energy Science, 3, 293–300, https://doi.org/10.5194/wes-3-293-2018, 2018.

Meyer Forsting, A. R., Troldborg, N., and Borraccino, A.: Modelling lidar volume-averaging and its significance to wind turbine wake measurements, Journal of Physics: Conference Series, 854, 012 014, https://doi.org/10.1088/1742-6596/854/1/012014, 2017.

Mizuno, T. and Panofsky, H. A.: The validity of Taylor's hypothesis in the atmospheric surface layer, Boundary-layer Meteorology, 9, 375–80, 375–380, https://doi.org/10.1007/BF00223388, 1975.

Newman, J. F. and Clifton, A.: An error reduction algorithm to improve lidar turbulence estimates for wind energy, Wind Energy Science, 2, 77–95, https://doi.org/10.5194/wes-2-77-2017, 2017.

Peña, A., Gryning, S.-E., and Mann, J.: On the length-scale of the wind profile, Quarterly Journal of the Royal Meteorological Society, 136, 2119–2131, https://doi.org/10.1002/qj.714, 2010.

Peña, A., Mann, J., and Dimitrov, N. K.: Turbulence characterization from a forward-looking nacelle lidar, Wind Energy Science, 2, 133–152, https://doi.org/10.5194/wes-2-133-2017, 2017.

Raach, S., Schlipf, D., Haizmann, F., and Cheng, P. W.: Three dimensional dynamic model based wind field reconstruction from lidar data, Journal of Physics: Conference Series, 524, 012 005, https://doi.org/10.1088/1742-6596/524/1/012005, 2014.

Reinwardt, I., Gerke, N., Dalhoff, P., Steudel, D., and Moser, W.: Validation of wind turbine wake models with focus on the dynamic wake meandering model, Journal of Physics: Conference Series, 1037, 072 028, https://doi.org/10.1088/1742-6596/1037/7/072028, 2018.

Sathe, A. and Mann, J.: A review of turbulence measurements using ground-based wind lidars, Atmospheric Measurement Techniques, 6, 3147–3167, https://doi.org/10.5194/amt-6-3147-2013, 2013.

Sathe, A., Mann, J., Barlas, T. K., Bierbooms, W., and van Bussel, G.: Atmospheric stability and its influence on wind turbine loads, Proceedings of Torque 2012, the Science of Making Torque From Wind, 2012.

Schlipf, D., Trabucchi, D., Bischoff, O., Hofsäss, M., Mann, J., Mikkelsen, T., Rettenmeier, A., Trujillo, J., and Kühn, M.: Testing of Frozen Turbulence Hypothesis for Wind Turbine Applications with a Scanning LIDAR System, Detaled Program, 2010.

Schmidt, B., King, J., Larsen, G. C., and Larsen, T. J.: Load validation and comparison versus certification approaches of the Risø dynamic wake meandering model implementation in GH bladed, European Wind Energy Conference and Exhibition 2011, Ewec 2011, pp. 249–254, 2011.

Simley, E., Angelou, N., Mikkelsen, T., Sjöholm, M., Mann, J., and Pao, L. Y.: Characterization of wind velocities in the upstream induction zone of a wind turbine using scanning continuous-wave lidars, Journal of Renewable and Sustainable Energy, 8, 013 301, https://doi.org/10.1063/1.4940025, 2016.

Sjöholm, M., Mikkelsen, T., Mann, J., Enevoldsen, K., and Courtney, M.: Time series analysis of continuous-wave coherent Doppler Lidar wind measurements, Iop Conference Series: Earth and Environmental Science, 1, 012 051 (6 pp.), 012 051 (6 pp.), https://doi.org/10.1088/1755-1315/1/1/012051, 2008.

Sonneschein, C. M. and Horrigan, F. A.: Signal-to-noise relationship for coaxial systems that heterodyne backscatter from the atmosphere, Applied Optics, 10, 1600–4, 1600–1604, https://doi.org/10.1364/AO.10.001600, 1971.

Taylor, G.: The spectrum of turbulence, Proceedings of the Royal Society of London Series A-mathematical and Physical Sciences, 164, 0476–0490, 1938.

Thomsen, K. and Sørensen, P.: Fatigue loads for wind turbines operating in wakes, Journal of Wind Engineering and Industrial Aerodynamics, https://doi.org/10.1016/S0167-6105(98)00194-9, 1998.

Thomsen, K., Madsen, H. A., Larsen, G. C., and Larsen, T. J.: Comparison of methods for load simulation for wind turbines operating in wake, Journal of Physics: Conference Series (online), 75, 012 072, https://doi.org/10.1088/1742-6596/75/1/012072, 2007.

Trujillo, J.-J., Bingöl, F., Larsen, G. C., Mann, J., and Kühn, M.: Light detection and ranging measurements of wake dynamics. Part II: two-dimensional scanning, Wind Energy, 14, 61–75, https://doi.org/10.1002/we.402, 2011.

Vermeer, L. J., Sørensen, J. N., and Crespo, A.: Wind turbine wake aerodynamics, Progress in Aerospace Sciences, 39, 467–510, https://doi.org/10.1016/S0376-0421(03)00078-2, 2003.

Vignaroli, A. and Kock, C. W.: UniTTe MC2 Nørrekær Enge Measurement System & Calibration report, 2016.

Wagner, R., Pedersen, T. F., Courtney, M., Antoniou, I., Davoust, S., and Rivera, R. L.: Power curve measurement with a nacelle mounted lidar, Wind Energy, 17, 1441–1453, https://doi.org/10.1002/we.1643, 2014.